7   Results

The previous chapter has described the physical characteristics of the individual study site locations. This chapter focuses on the factors that are relevant to the *Bilate* watershed as a whole, as well as to the geomorphological units:

- Rainfall-runoff analysis has been carried out for the watershed.
- Illustration of the erosion and soil erosion damages is first categorized for the entire watershed and is then disaggregated to the study sites and geomorphological units. The geomorphological unit associated with each study site has been added in brackets.
- Soil and soil sediments samples are described in relation to soil type units determined by FAO.

A Land Cover Class Index has been designed and is presented in relation to the geomorphological units and the watershed.

7.1   Rainfall - Runoff Analysis

7.1.1   Rainfall

Precipitation is generally dependant on altitude in the Lake *Abaya-Chamo Basin* (BEKELE 2001) and thus, is spatially variable across the watershed. The modelled annual precipitation has its highest value of ~2,000 mm in the *Western Ethiopian Highlands* and lowest value of 750 mm in the *Rift Valley*, whereas in the *Valleys and Basin* precipitation ranges from 1,100 mm to 1,950 mm (fig. 53).

7.1.1.1 Rainfall Variability

Remarkable precipitation data of meteorological stations (fig. 52) in the watershed highlight the high variability throughout the time period from 1970-1996 (tab. 9).

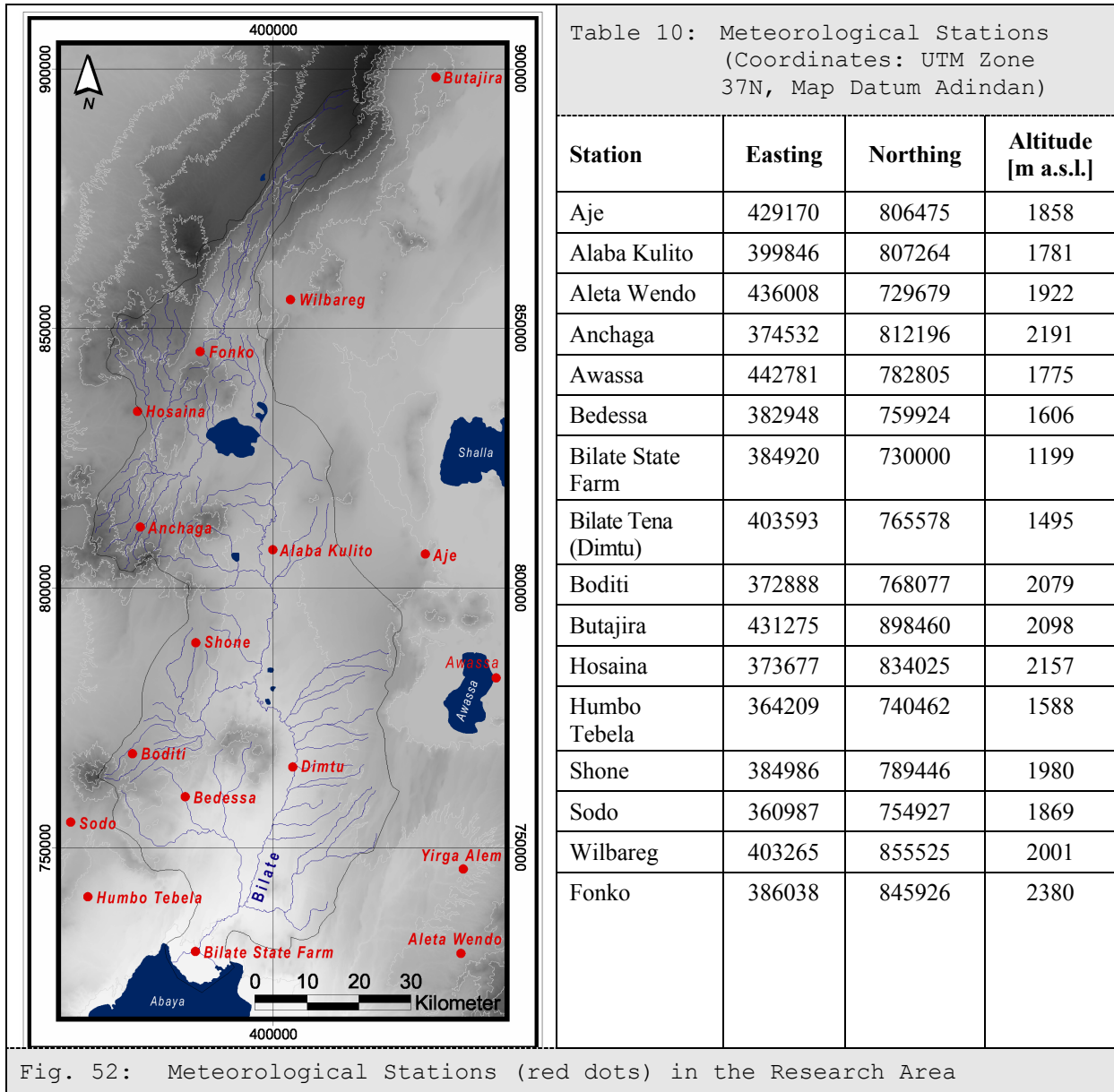| Table 9: Remarkable annual precipitation data			
	minimum annual rainfall	maximum annual rainfall	standard deviation
Western Ethiopian Highlands	852 mm (Hossaina)	1732 mm (Hossaina)	220 mm/a n = 27
Valleys and Basin	1,100 mm (modelled)	1,950 mm (modelled)	no meteorological station
Rift Valley	490 mm (Bilate State Farm)	1074 mm (Bilate State Farm)	166 mm/a n = 27

Table 10: Meteorological Stations (Coordinates: UTM Zone 37N, Map Datum Adindan)			
Station	**Easting**	**Northing**	**Altitude [m a.s.l.]**
Aje	429170	806475	1858
Alaba Kulito	399846	807264	1781
Aleta Wendo	436008	729679	1922
Anchaga	374532	812196	2191
Awassa	442781	782805	1775
Bedessa	382948	759924	1606
Bilate State Farm	384920	730000	1199
Bilate Tena (Dimtu)	403593	765578	1495
Boditi	372888	768077	2079
Butajira	431275	898460	2098
Hosaina	373677	834025	2157
Humbo Tebela	364209	740462	1588
Shone	384986	789446	1980
Sodo	360987	754927	1869
Wilbareg	403265	855525	2001
Fonko	386038	845926	2380

Fig. 52: Meteorological Stations (red dots) in the Research Area

The inter-annual variability of precipitation totals is high. VAN ROOY (1965) designed a rainfall anomaly index to interpret temporal rainfall anomalies. Based on VAN ROOY (1965) BÄRRING & HULME (1991) calculate the standardized rainfall as:

$$RAI_{ij} = \frac{P_{ij} - \overline{P_i}}{s_i} \qquad (1)$$

RAI_{ij} = normalized annual, seasonal or monthly rainfall total for station i

P_{ij} = corresponding annual rainfall total

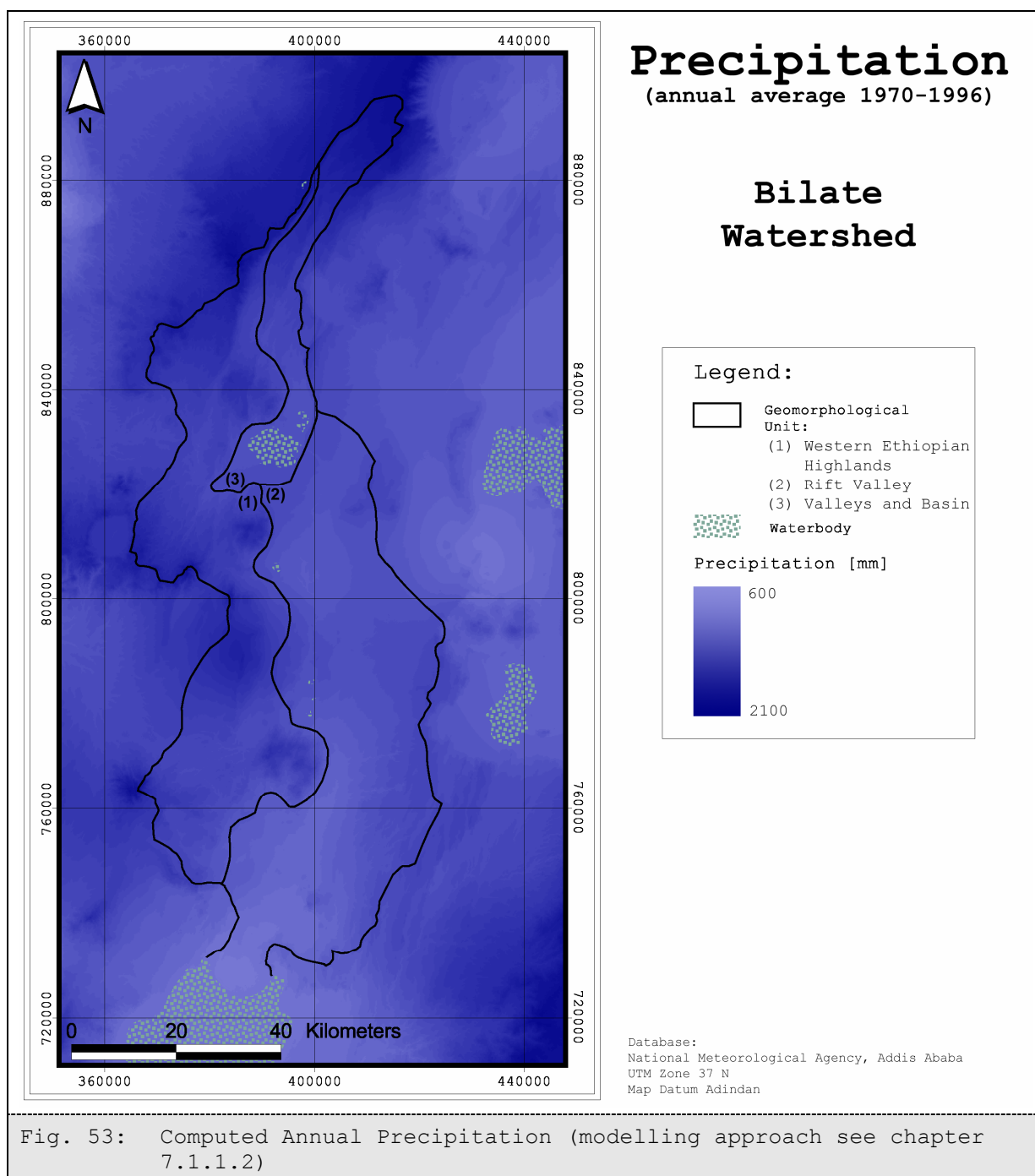P_i = mean rainfall total for station i during the reference period

s_i = standard deviation of the rainfall total during the same reference period

(i = station; j = time period)

FÖRCH (1989) gives some indication of the rainfall anomaly index of Ethiopia. While the index is lowest (<0.1) in the centre of the Western Highlands of Ethiopia, the index is increasing in the southwest and the northwest (>0.5). The watershed of the *Bilate* has an index between 0.1 and 0.2.

Figure 53 displays the annual average precipitation (1970-1996) in the watershed. Precipitation totals differ from ~600 mm/a in the southern part of the *Rift Valley* and reach their maximum of ~2,100 mm/a in the northern regions of the *Western Ethiopian Highlands* and the *Valleys and Basin*.

Fig. 53: Computed Annual Precipitation (modelling approach see chapter 7.1.1.2)

Fig. 54:   Mean Annual Precipitation Variability of Selected Meteorological
           Stations (line graph was used for better illustration of the
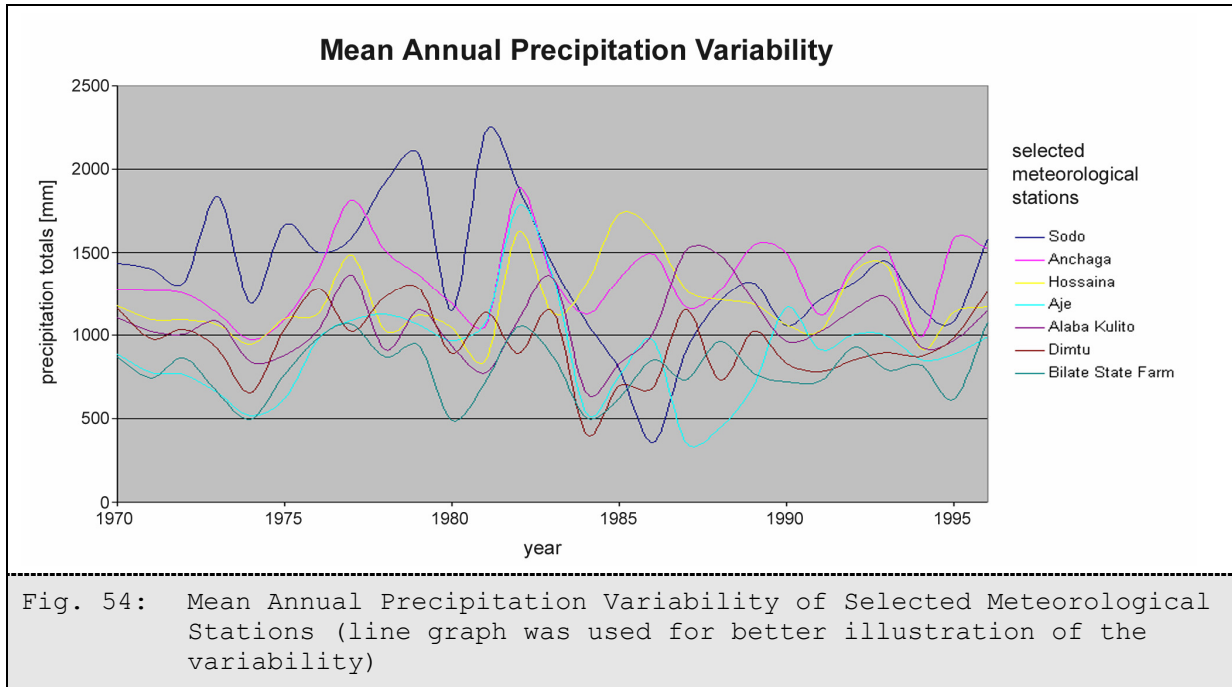   variability)

Figure 54 shows charts of seven selected meteorological stations within the research area. General trends, such as minimal precipitation totals in 1974, 1982 or 1993 can be detected, but are seldom consistent between stations. Moreover, the inter-annual precipitation totals do not correspond with the climate variability caused by the El-Niño Southern Oscillation (ENSO) effect. Figure 55 exemplarily shows the relationship between the annual precipitation totals of the meteorological stations *Hossaina* (*Western Ethiopian Highlands*) and *Alaba Kulito* (*Rift Valley*) and the El Niño / La Niña events represented by the ENSO index (CDC, 2005). Both charts show some degree of consistency between the station totals and El Niño / La Niña events. High precipitation totals coincide with El Niño events, but this is also true for La Niña events and lower annual precipitation totals. Thus, the relationship between ENSO and precipitation is often conflicting and does not show a consistent pattern.

Fig. 55:   El Niño Events plotted against Annual Precipitation
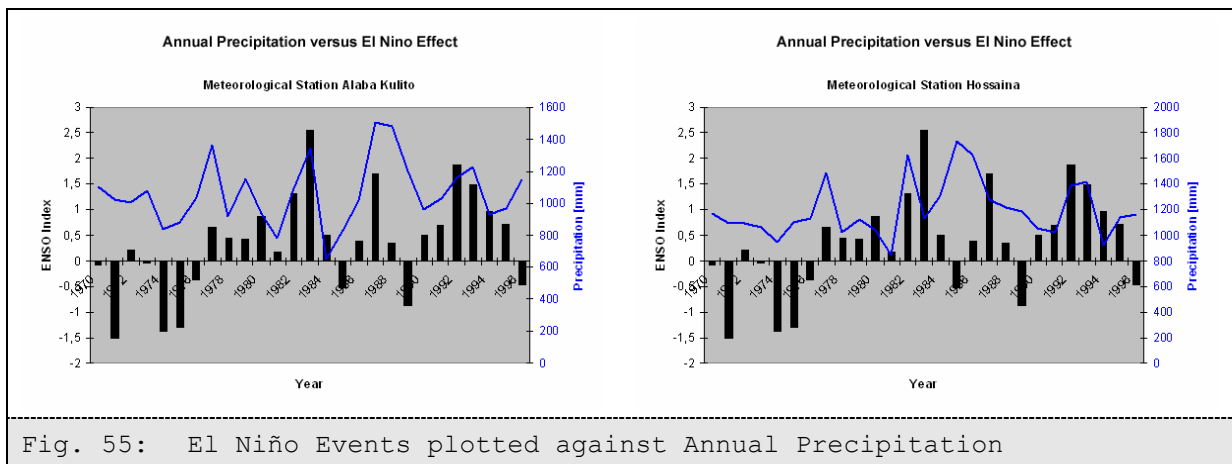
7.1.1.2 Rainfall Totals

The analysis of the distribution of the average monthly precipitation totals shows that the dependence on altitude is variable throughout the year. The average monthly precipitation totals for a period of 26 years (1970-1996) can be described by an exponential equation for 9 months. For January the equation is linear, while no correlation between precipitation and altitude could be detected for October and November (tab. 11). The correlation is not significant for January, April, June and December ($\alpha < 0.05$, n = 16). These are the dry season months and the transition period from small to the large rainy season.

The dependence of precipitation on altitude is more pronounced in the rainy season than in the dry season. But in years of less precipitation totals the dependence on altitude is stronger than in years of high precipitation totals (THIEMANN & FÖRCH, 2005). The adequateness of the equations below has been verified by comparing the results of modelling based on these data with observed data from the meteorological stations. The intra-monthly variability is not considered in these results, however high variability is known to exist.

Table 11:	Monthly Average Precipitation versus Altitude			
January	$P = 0.0128 \bullet alt + 9.495$	$r^2 = 0.28$	(n=16)	$\alpha > 0.05$
February	$P = 0.0123 \bullet alt^{1.111}$	$r^2 = 0.55$	(n=16)	$\alpha < 0.05$
March	$P = 0.011 \bullet alt^{1.2193}$	$r^2 = 0.51$	(n=16)	$\alpha < 0.05$
April	$P = 1.1121 \bullet alt^{0.6431}$	$r^2 = 0.16$	(n=16)	$\alpha > 0.05$
May	$P = 0.2778 \bullet alt^{0.8328}$	$r^2 = 0.57$	(n=16)	$\alpha < 0.05$
June	$P = 1.119 \bullet alt^{0.6264}$	$r^2 = 0.40$	(n=16)	$\alpha > 0.05$
July	$P = 0.2678 \bullet alt^{0.8385}$	$r^2 = 0.49$	(n=16)	$\alpha < 0.05$
August	$P = 0.0011 \bullet alt^{1.5783}$	$r^2 = 0.75$	(n=16)	$\alpha < 0.05$
September	$P = 0.0272 \bullet alt^{1.1217}$	$r^2 = 0.74$	(n=16)	$\alpha < 0.05$
October	no correlation found			
November	no correlation found			
December	$P = 0.0009 \bullet alt^{1.3791}$	$r^2 = 0.27$	(n=16)	$\alpha > 0.05$
	P = precipitation [mm/month]; alt = altitude [m a.s.l.]			

Daily precipitation data are available for the years 1990 to 2002 from five meteorological stations. Moreover, data are available for an additional three stations for 2001 and 2002. However, these data are insufficient for spatial modelling or analyzing time series characteristics for the entire watershed. Therefore they have only been used to fill data gaps in time series of the monthly precipitation data.

Hourly precipitation data are only available for the meteorological stations *Sodo* and *Hossaina*. These data are also insufficient for any spatial and temporal analysis, but they provide information about the very high daily and hourly precipitation variability.

7.1.1.3 Rainfall Intensity

Next to precipitation totals, rainfall intensity is of high interest. Analysis of hourly rainfall data of the meteorological station *Hossaina* shows that rainfall events are mainly of short duration and high intensity. During the dry season, the events have durations of one or sometimes two hours and the event totals range between 0.6 mm/h and 11 mm/h (e.g. in February 2001). For three selected days in the dry season of 2001 the standard deviations are between 1.63 and 2.25 mm/h. While rainfall events have been recorded for 8 days throughout February, the maximum rainfall was only 18.1 mm/d (tab. 12).

During the rainy season month of September rainfall events have a duration ranging from one to five hours and the maximum rainfall during a storm event is generally at the beginning. The amount of hourly rainfall is between 0.3 mm and 17.5 mm, but the maximum intensities of the rainfall events with different lengths are not changing distinctively. In September 2001 it rained on 17 days. Three days have been selected in order to demonstrate the intensity of rainfall during the rainy season. Table 12 illustrates the differences in intensities of rainfall events in the rainy and dry seasons. On average the standard deviation is smaller in the rainy season than in the dry season, whereas the hours of rainfall events are generally longer in the rainy season.

Table 12: Descriptive Statistic of Hourly Precipitation for Three Selected Days in Dry and Rainy Season (Station *Hossaina*)					
	dry season			rainy season		
Date	07.02.2001	08.02.2001	09.02.2001	07.09.2001	08.09.2001	09.09.2001
Mean	0.46	0.33	0.75	0.92	0.33	0.01
Standard Deviation	2.25	1.63	1.91	2.90	0.11	0.06
Minimum	0	0	0	0	0	0
Maximum	11.0	8.0	8.5	14.1	0.5	0.3
Hours of Rainfall	1	1	7	8	3	1
Sum	11.0	8.0	18.1	22.2	0.8	0.3
Count	24	24	24	24	24	24

A rainfall-intensity-index (RII) has been designed for this study, as intensity data are not available for the research area. Rainfall intensity is one input parameter for modelling actual erosion and soil erosion risk and thus it is essential to predict. The RII provides a mean

to assess the differences in spatial and temporal rainfall intensity. The RII is derived from the quotient of the maximum rainfall totals of one day within a month to the rainfall totals of the same month. This gives a standardized and thus comparable value for all meteorological stations and therefore a relatively good indication of the spatial and temporal variation of rainfall intensity.

$$RII = \frac{N_{\max,[day]}}{N_{total}}[month] \qquad\qquad (2)$$

Figure 56 demonstrates the rainfall-intensity-index for the three geomorphological units. The index for the watershed is displayed in figure 57.

The graphs represent the rainfall intensity index plotted against the frequency. The x-axis shows the intensity index: '0' stands for no rainfall, '1' means that only one single rainfall event took place within the particular month. The y-axis shows the month, while the clusters display the relative potential frequency of the rainfall intensity index.

All four graphs display similar distributions of the index value and its temporal occurrence. However, the ratios are different throughout the year. The index is higher in the *Rift Valley* than in the *Valleys and Basin*, while the index is smallest in the *Western Ethiopian Highlands*. Also, the index is distinctly higher in the dry season than in the rainy season in all three geomorphological units, while the highest absolute values occur in the *Rift Valley*. Exceptional are the values in November in the *Valleys and Basin* caused by the limited amount of data available for computation.

In the *Western Ethiopian Highlands* the index ranges between 0.4 and 0.7 from November to February, while the maximum relative frequency is in January reaching 60-70%. From March to September the index is between 0.05 and 0.35 and here the maximum relative frequency reaches 60-70% in August. From September to November the index is slightly higher between 0.3 and 0.4 with maximum relative frequency of 40-50%.

Three temporal clusters of high intensity indices can also be differentiated in the *Rift Valley*. The index ranges from 0.4 to 0.7 from mid-October to mid-March, whereas two maxima exist with relative frequency of 40% and 50%, respectively. From mid-March to mid-August the index computes to values between 0.15 and 0.35. Here the maximum of the relative frequency reaches 60-70% in May. The third cluster is from mid-August to mid-October. Values are between 0.3 and 0.4 and the maximum of the relative frequency reaches 50-60% in October.

Average (26 y.) Monthly Rainfall Intensity in the Western Ethiopian Highlands

Average (26 y.) Monthly Rainfall Intensity in the Rift Valley

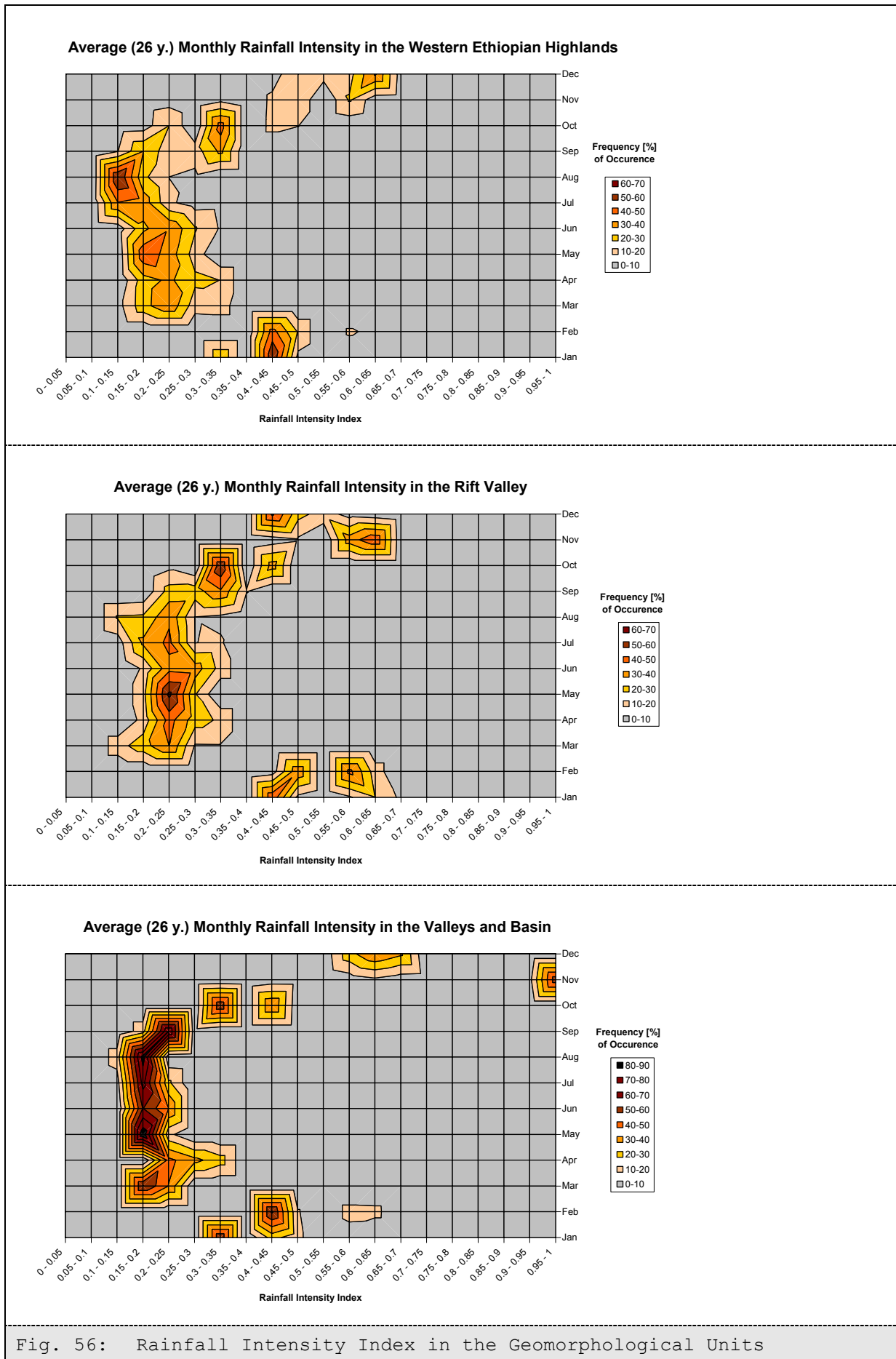**Average (26 y.) Monthly Rainfall Intensity in the Valleys and Basin**

Fig. 56:   Rainfall Intensity Index in the Geomorphological Units

In the *Valleys and Basin* three different clusters of high intensity indices can be separated as well. The values in November are ignored (see above). From November to December the index is between 0.55 and 0.75 and the relative frequency reaches 30-40% where its maximum is at 0.65. Another cluster has values from 0.3 to 0.5 for the months of January, February and October. Two peaks compute to 0.35 and 0.45 with maximum relative frequencies in February (60-70%) and October (50-60%). For the months March through September the index ranges between 0.1 to 0.35 and the maximum relative frequencies are 0.2 with three peaks in March (50-60%), May (80-90%) and August (80-90%).

Figure 57 displays the Rainfall Intensity Index for the *Bilate w*atershed: the distribution of the RII is similar than for the individual geomorphological units, but levelled since the index shows the average of the indices of the three geomorphological units.

Fig. 57:   Rainfall Intensity Index in the *Bilate* Watershed
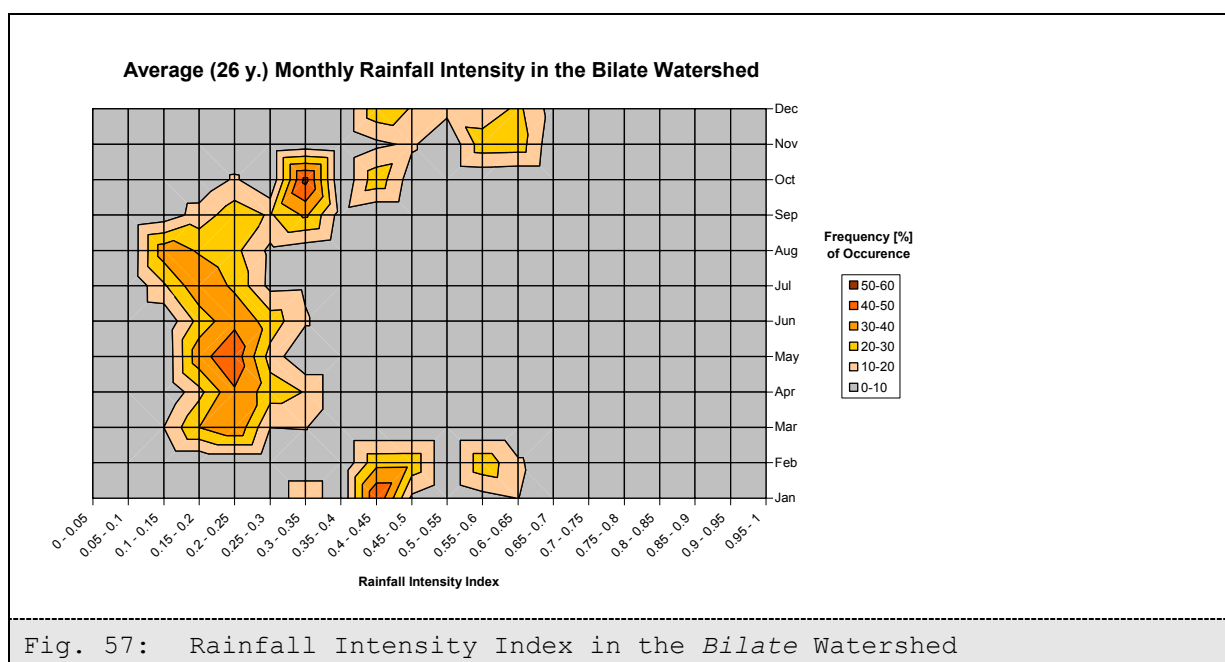
7.1.2   Runoff

Monthly and daily discharge data exist for five gauging stations in the study area.

Table 13: River Gauging Stations of the Watershed

Gauging Station	River	Geomorphological Unit
Weira	*Weira*	*Valleys and Basin*
Batena	*Bilate*	*Western Ethiopian Highlands*
Guder	*Guder*	*Western Ethiopian Highlands*
Alaba Kulito	*Bilate*	*Rift Valley*
Bilate Tena (Dimtu)	*Bilate*	*Rift Valley*

The time series of all gauging stations cover different periods and have data points missing throughout their data sets. The larger gaps (tab. 14) cannot not be closed by including calculated discharge data derived from daily values, since comparisons between monthly totals of daily data differ from provided monthly data. Also, standard procedures for filling missing discharge data cannot be utilised. No correlations between corresponding gauging stations could be determined. Since full data sets exist only for the twelve month in 1992, the five gauging stations can only be compared for that time period. However, necessity of filling gaps in runoff time series is evident for probabilistic evaluation of reliable hydrographs (GYAU-BOAKYE & SCHULTZ, 1994).

Table 14: Gaps in Daily Discharge Data of Gauging Station *Dimtu* (1986)

	July	August	September	October	November	December
1	114.769	-	-	-	55.533	1.766
2	103.095	-	-	-	52.791	1.344
3	96.219	132.221	-	-	45.925	1,86
4	89.657	-	-	-	-	1.503
5	85.868	-	-	-	-	1.344
6	87.119	-	-	-	-	27.773
7	78.614	-	-	-	-	32.069
8	75.146	-	-	-	-	34.713
9	74.014	-	-	-	-	32.069
10	71.783	-	80	-	-	28.362
11	71.783	145.973	-	-	-	26.057
12	137.271	132.221	-	101.694	-	1.503
13	124.083	-	-	96.219	-	1.126
14	111.771	-	-	90,945	-	1.344
15	105.935	-	-	87.119	-	1.196
16	104.508	-	-	84,629	-	0.934
17	104.508	-	-	82.187	-	0.713
18	164.47	-	-	78.614	-	-
19	236.536	-	-	71.783	-	-
20	206.048	-	-	69.597	-	-
21	186.561	-	-	68.522	-	-
22	170.31	-	80	74.014	-	-
23	156.893	-	-	76.291	-	-
24	149.554	-	-	87.119	-	-
25	142.449	-	-	68.522	1.766	1.766
26	135.574	-	-	64.33	-	1.675
27	132.221	-	-	62.3	-	1.588
28	166.401	-	132.221	60.313	1.675	1.344
29	283.54	-	-	59.336	1.503	1.344
30	174.28	-	-	58.369	1.503	1.344
31	160.652	-		57.414		1.344

[m³/s]

The graph (fig. 58) shows generally bimodally distributed discharge totals and highlights the extreme inter-annual variability of discharge volumes. Some hydrographs clearly demonstrate the characteristically bimodal distribution. However, monthly maxima and minima do not always occur in the same month. In general, a small peak in March to June is alternating with a relative minimum in June/July and a main peak in August and September. The lowest and highest discharge volumes were 181 and 567 mio m³ in 1991 and in 1996. The standard deviation is 108 mio m³/a. The Ministry of Water Resources provides discharge data only in the units [m³/s] or [mio m³/time].

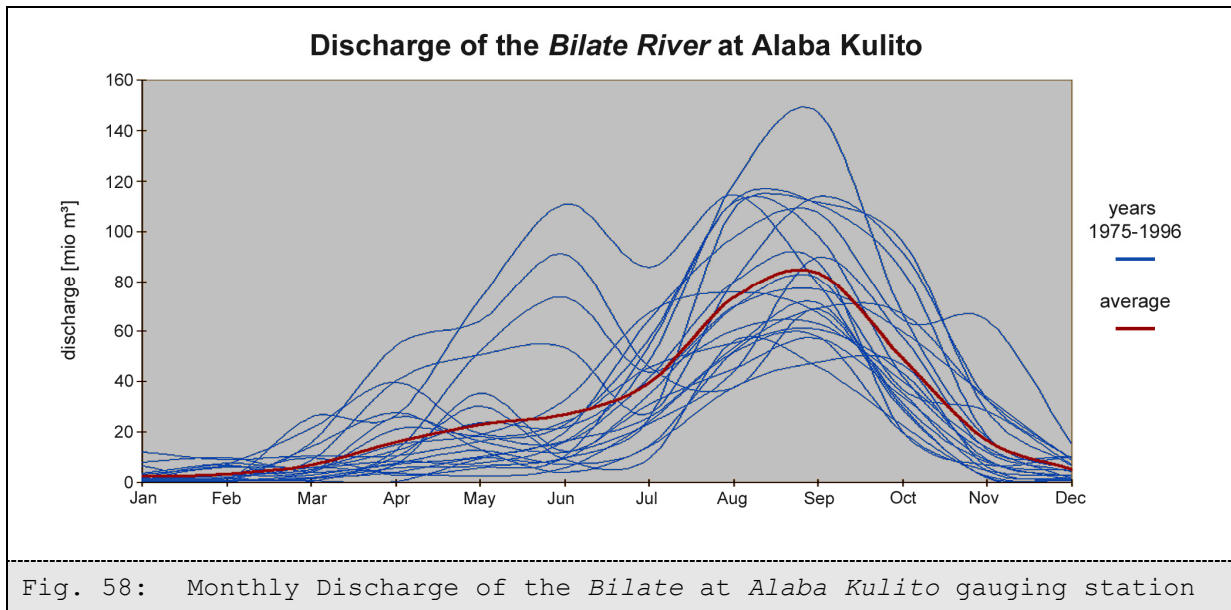**Discharge of the *Bilate River* at Alaba Kulito**

Fig. 58:   Monthly Discharge of the *Bilate* at *Alaba Kulito* gauging station

Table 15:   Descriptive Statistic of Average (1972-2000) Monthly Discharge at *Alaba Kulito* gauging station [mio m³]

	mean	max	min	std. dev.	n
Jan.	2.71	12.14	0.45	2.75	30
Feb.	3.19	9.07	0.29	2.87	30
Mar.	6.22	25.70	0.34	6.23	30
Apr.	14.56	54.39	0.42	13.62	30
May	20.36	72.93	2.58	18.28	29
Jun.	23.76	112.67	4.13	26.63	29
Jul.	38.13	85.70	9.60	18.83	29
Aug.	74.19	130.35	30.37	30.20	29
Sep.	85.46	147.06	35.85	28.24	29
Oct.	53.68	98.78	19.61	24.22	29
Nov.	17.91	65.39	1.83	15.88	29
Dec.	4.80	15.66	0.59	3.83	28

At the gauging station *Tena Bilate (Dimtu)* a complete annual dataset only exists for 8 years and thus, meaningful statements concerning discharge volumes cannot be made. Comparison of inter-annual discharge totals shows that the average annual volume at *Alaba Kulito* (346 mio m³/a) is distinct smaller than that at *Tena Bilate (Dimtu)* (518 mio m³/a). In comparison, the watersheds associated with the gauging stations *Alaba Kulito* and *Tena Bilate (Dimtu)* are 1,982.6 km² and 3,877.2 km², respectively. The watershed south of *Tena Bilate (Dimtu)* has no gauging station.

Discharge data of the other gauging stations *Weira*, *Batena* and *Guder* are also insufficient for a meaningful analysis (see fig. 59). For *Weira* only some data are available within the time period from 1983 to 2000. For this watershed (500.1 km²) the average annual discharge was calculated as 206 mio m³ (SD=84 mio m³, n=14). At *Batena* (size of associated watershed is 137.1 km²), discharge of 12 years was recorded and the average annual discharge amounts to 566 mio m³ (SD=1022 mio m³, n=9). Here, the small number of available data led to the very high standard deviation. It could not be verified whether the high average annual discharge rate is actually occurring or due to some extraordinary events or due to measurement errors. For the station *Guder* data are available for 13 years. Here, the average discharge is 55.7 mio m³/a (SD=31 mio m³, n=11) and the watershed has an extent of 97.7 km².

Fig. 59:   Average Discharge of the *Bilate* and Tributaries
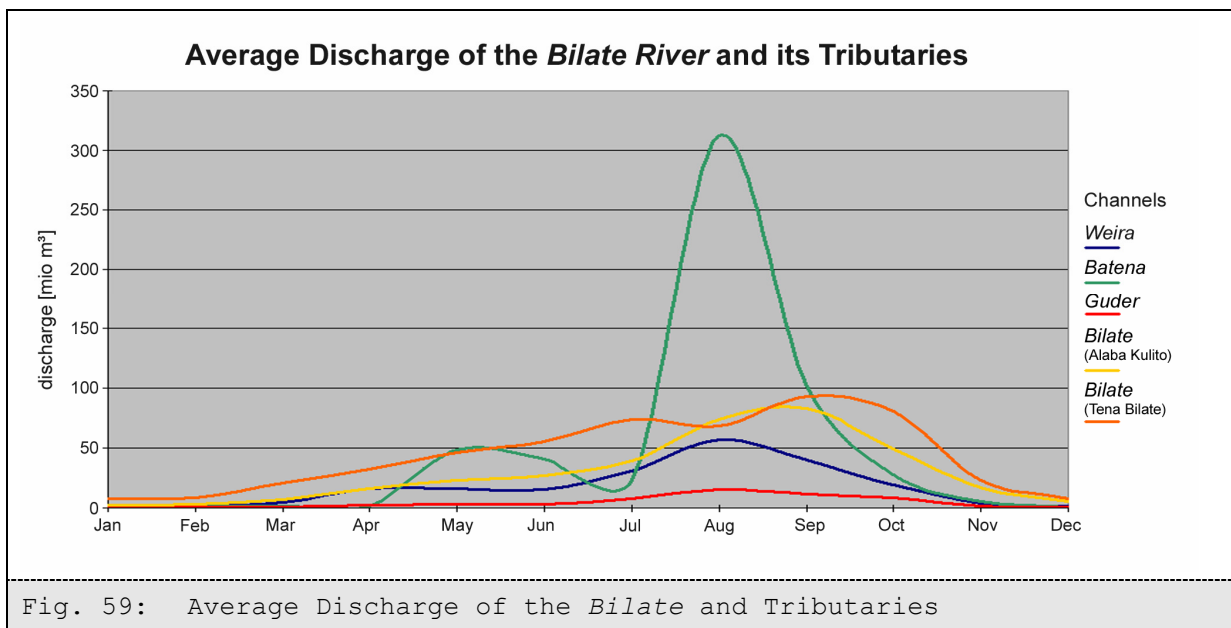
7.1.3   Rainfall-Runoff

Average (1970-1996) monthly rainfall volumes computed for the watershed that are associated with the gauging station *Tena Bilate (Dimtu)* vary from 51.4 mio m³ (27 mm/m²) in February to 295.3 mio m³ (155 mm/m²) in August. *Tena Bilate (Dimtu)* gauging station is recording discharge from 3,877.2 km², which is ~70% of the entire watershed.

	mean	max	min	std. dev.	n
Table 16: Descriptive Statistics of average rainfall volumes associated with *Tena Bilate (Dimtu)* Gauging Station [mio m³]					
Jan.	40.62	63.55	27.52	6.0	26
Feb.	61.33	99.60	37.55	10.2	26
Mar.	109.50	174.54	88.53	11.7	26
Apr.	141.96	206.89	113.93	15.5	26
May	148.42	215.96	115.08	12.8	26
Jun.	121.43	205.58	80.83	17.4	26
Jul.	149.91	229.84	115.38	17.0	26
Aug.	155.86	314.23	91.15	24.7	26
Sep.	142.82	225.02	100.64	19.9	26
Oct.	82.98	105.59	68.74	7.4	26
Nov.	30.58	46.79	18.06	5.3	26
Dec.	27.13	50.19	18.70	4.7	26

Average rainfall data for the watershed of the gauging station *Batena (WEH)* shows extremely variable intra-annual volumes. For the time period of 26 years they vary from 1.1 mio m³ (8 mm/month) in February to 36.3 mio m³ (264 mm/month) in August (mean=16.74, SD=1.35, n=12). Discharge totals for 1992 can be compared with the precipitation volume and show some, but not distinct correlation (see exemplary fig. 60).

Fig. 60: Discharge Volumes versus Precipitation Volumes at *Batena* Gauging Station in 1992
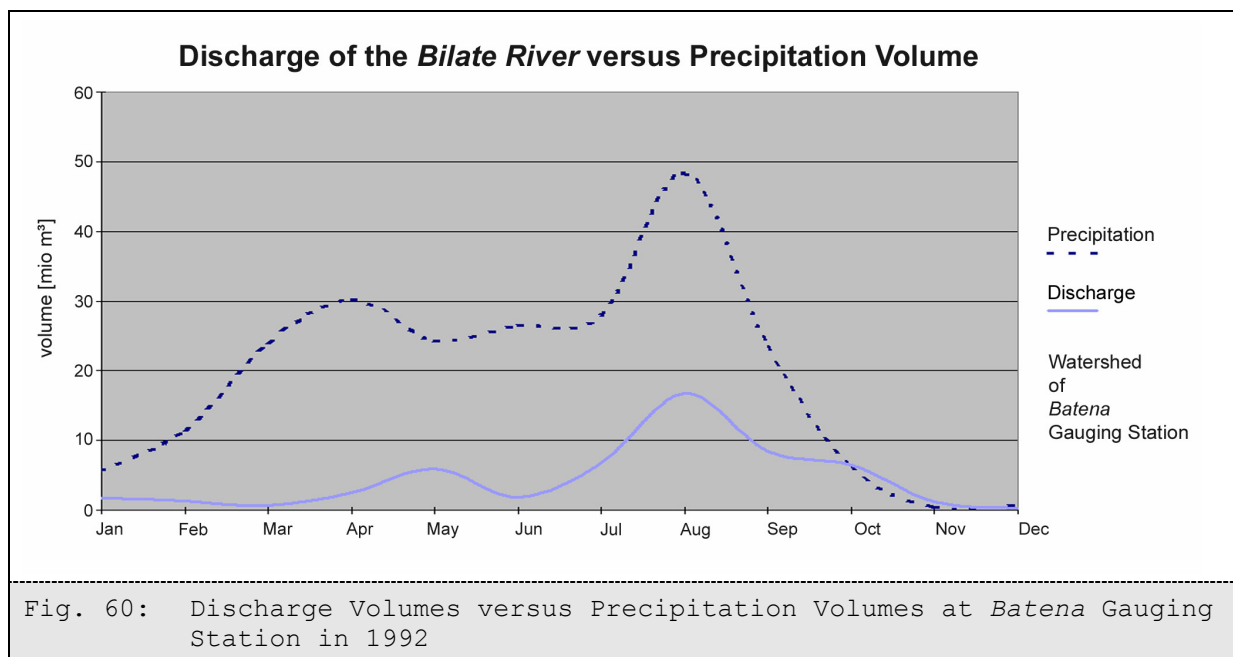
In general, precipitation volumes of selected watersheds are much higher than the volumes of related discharge. The characteristic bimodal distribution of discharge throughout the year can be observed in the watersheds associated with both *Batena* and *Bilate Tena (Dimtu)* gauging stations. Data gaps for all other gauging and meteorological stations made additional comparisons impossible. However, discharge of the *Bilate* is reacting to precipitation with a time lag of approximately one month in the end of the dry season at *Batena* and *Bilate Tena (Dimtu)*. In the rainy season the time lag is missing entirely at *Batena*, whereas at *Bilate Tena (Dimtu)* the time lag is at least one month (fig. 61).

The investigation of rainfall-runoff relation was not intensified, since the above mentioned results show clearly the problematic of (un-)reliable data in this watershed. Discharge data often cannot be related to corresponding rainfall data. For instance in figure 61 the discharge volumes from five month (Jan. to May) show small values (0-10 mio m³), whereas the precipitation volumes computed for the related watershed vary from 50 (Jan.) to 330 (Apr.) mio m³. Even under consideration of high evapotranspiration (up to 2,000 mm/a) and retention capacity in the watershed the monthly input volumes are in maximum 30 times higher than the output volumes. Additionally, figure 59 highlights for the month August higher discharge volume at *Batena* discharge gauging station than at the more downstream located *Alaba Kulito* gauging station. And the most downstream located gauging station *Tena Bilate* experiences the smallest discharge values. That is impossible, since only small abstraction systems are known in that area.

7.2 Erosion and Soil Erosion Damages

In general, erosion and soil erosion damages occur in various shapes and sizes in the *Bilate* watershed. However, the different erosion and soil erosion forms are not distributed uniformly across the watershed. While on- and off-site damages from sheet and rill erosion are recorded across the watershed, small channels, gullies, badlands and degraded barren lands only occur in some areas. The different frequencies and appearances of the various erosion and soil erosion damages have been recorded on the ground at the study sites and detected on satellite images and aerial photographs at larger scales. Maps of erosion and soil erosion damages, soil conservation measures and anthropogenic impacts on the landscape have been developed for the study sites (see appendices 14.3).

7.2.1 Sheet erosion

Since sheet erosion can hardly be detected directly, indirect indicators such as fans in agricultural fields without corresponding rill or gully erosion, tillage edges or severe majority of stones or coarse grains allow assessment of sheet erosion in the field. These damages further downhill occur across the watershed and thus, indicate area-wide processes of sheet erosion. Figure 61 shows a fan in an agricultural field without corresponding erosion damages.

Fig. 61:   Off-Site Damages due to Sheet Erosion

7.2.2 Rill Erosion

Damages caused by rill erosion (fig. 62) coincide with intensive cultivation. Rills have only been detected in the rainy season because livestock movement during the dry season levels the micro-relief of the fields. The development of rill erosion damages appears to be independent of different crop cultivation. While rill erosion damages can be detected on all slopes; the steeper and longer the slopes the higher the frequency and incision of rills.

A detailed measurement of shape and frequency of rills was carried out on a small test plot in the study site *Ana (WEH)*. The plot was approximately 20 x 25 m² and had an average slope of 20°. The micro relief, i.e. length, cross section and frequency of rills, has been recorded before and after a single rainstorm event (17.08.2002, 23.6 mm/d, recorded at *Fonko* meteorological station). Differences in frequency, cross section and length of the rills before and after the storm event indicate a volume loss of 4.3 m³, which is equivalent to soil loss of ~0.8 cm for this single storm event.

Fig. 62:   Rill Erosion in the Western Ethiopian Highlands

In all four study sites in the *Western Ethiopian Highlands*, the rills reach a maximum depth of 15-20 cm. All sites show a high diversity of rill shapes and occurrences on agricultural fields. Most of the rills do not lead into any channels, but develop small fans further downhill (fig. 62, left picture). Steep and long slopes are the exception, however, as concentrated surface runoff in the rills develop small channels or sometimes gullies. These are tributary to the drainage system (fig. 62, right picture; fig. 63).

Fig. 63:   Rill Erosion on Long Slopes

In the study sites *Sedebo (RV), Bedesa (RV)* and *Dimtu (RV)* damages from rill erosion are very rare. Only in *Sedebo (RV)* some rills have been detected on ploughed fields. The study area *Agega (WEH/RV)* shows both: high appearance of damages from rill erosion in the headwater areas and hardly any damages in the alluvial zone.

In the geomorphological unit *Valleys and Basin* similar damages from rill erosion like in the *Western Ethiopian Highlands* appear. Especially in the southern part of this unit, where land-use is agricultural, damages were recorded. In the northern part of the unit damages from rill erosion are seldom.

7.2.3 Gully Erosion

Gullies occur in all study sites in different shapes and dimensions. Most gullies of the study sites *Ana (WEH), Doyancho (WEH), Hage (WEH)* and in the headwater area of *Agega (WEH/RV)* develop where surface runoff is concentrated either on ploughed fields or on grasslands and forest, respectively (fig. 64).

Fig. 64:   Gullies on Steep Slopes and Agricultural Land

These gullies are mostly v-shaped and sometimes show a high density of shrub vegetation at their rims. Gully width at the top sometimes reaches more than 8 m, whereas depth varies strongly from 1 to 60 meters. In some cases, like in *Ana (WEH)* watershed, several gullies form a gully system which affects a large area. The occurrence of gullies or gully systems in the study sites of the *Western Ethiopian Highlands* is dependent on relief position, slope gradient and on land use: gullies occur often at convex profile and concave plane relief curvature in combination with moderate to steep slopes and most significantly in association with eucalyptus plantations. Some extremely large gullies exist in *Doyancho (WEH)* study site that extend some 200 m horizontally and have a maximum depth of 60 m. These kinds of gullies are present intermittently across the *Western Ethiopian Highlands* (fig. 65).

Fig. 65:   Gullies at Different Relief Positions

In contrast to the *Western Ethiopian Highlands*, the appearances of gullies in the *Rift Valley* are significantly different. Ephemeral or inactive gullies are present on the large fields of the *Bedesa (RV)* watershed and the private farms at its centre. Large gullies are concentrated parallel to channels and develop barren degraded areas (fig. 66). Such concentration of gullies has been mapped in detail in the study area *Dimtu (RV)* as well. Gullies in the *Rift Valley* are u-shaped and never deeper than four to five meters, whereas incision is of high depth and little width. Secondary incision has been recorded at study site *Dimtu (RV)*.

Fig. 66:   Gullies at Study Area *Dimtu*
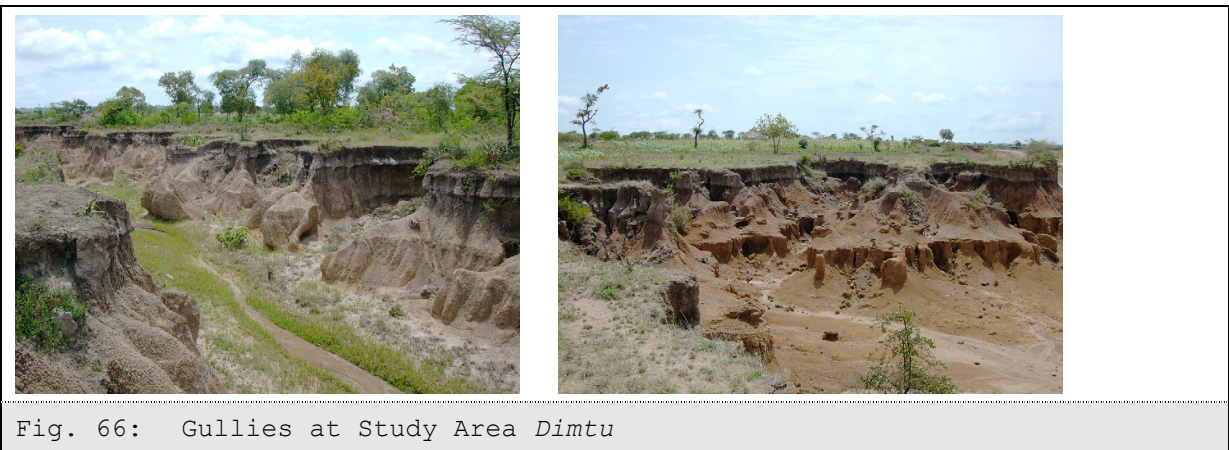
An additional type of gully system occurs in the transition zone from the *Western Ethiopian Highlands* to the *Rift Valley*. Here, the gullies are located on moderate to steep slopes and are extending into almost flat areas. The gully bottoms are generally v-shaped, instead of flat and show often secondary incision. Thus, while this does not lead to the development of large degraded areas, gully systems do develop across all slopes gradients (fig. 67).

Fig. 67:   Gully System in Transition Zone (*WEH/RV*)

In the *Valleys and Basin* geomorphological unit, gullies with v-shaped cross sections have been found on moderate as well as steep slopes. The development of these gullies is associated with eucalyptus cultivation.

7.2.4   Badland Erosion

The transition from clusters of gullies or high frequency of rills to developed badlands is not uniform in the *Bilate* watershed. Although badlands tend to develop within all geomorphological units, they usually occur at different relief positions. In the study site *Agega (WEH/RV),* badlands have formed on steep slopes between the *Western Ethiopian Highlands* and the *Rift Valley*. In headwater areas, gully formation generally coincides with eucalyptus cultivation in association with convex profile relief elements on moderate to steep slopes. The lower realms of these badlands often transform into gullies, which are tributary to the nearest channel. A similar spatial pattern has been observed in the headwater areas of the *Hage (WEH), Doyancho (WEH)* and *Ana (WEH)* study sites and in the *Valleys and Basin* geomorphological unit. The extents of the badlands always relates to the intensity of the utilisation of eucalyptus plantation (fig. 68).
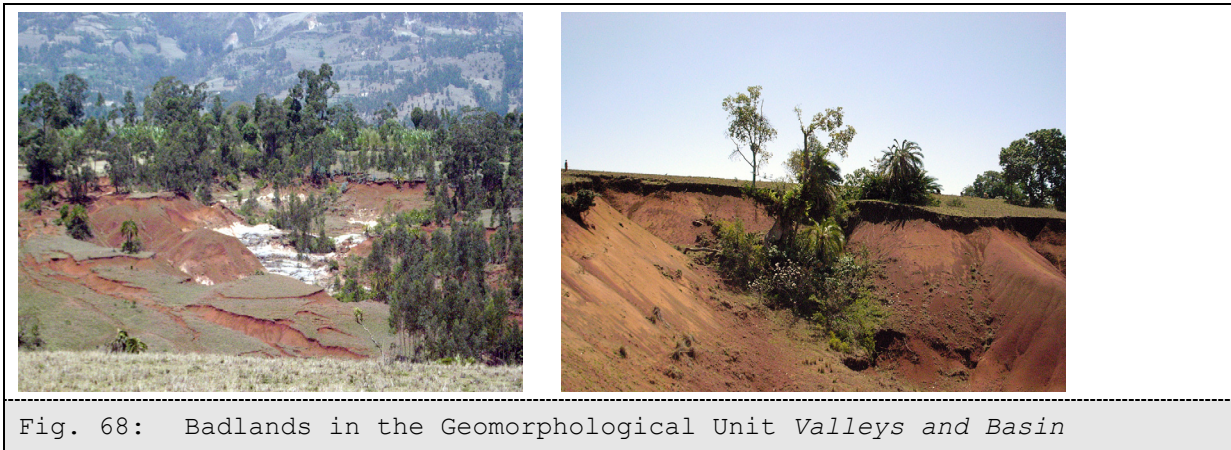
Fig. 68:   Badlands in the Geomorphological Unit *Valleys and Basin*

The study site *Sedebo (WEH/RV)* shows badlands in the transition zone to the *Rift Valley*. These areas are covering at least 1/3 of the study site. Presently they are closed for pasture and agriculture and vegetation is recovering and stopping further erosion (fig. 69, left picture). But wherever secondary incision started, the areas are neither treated mechanically to prevent erosion nor does the vegetation stabilize the rims of the badlands or gullies sufficiently (fig. 68, right picture). These deep incisions cause severe off-site damages at the outlet of the study site (fig. 70).

Fig. 69:   Vegetation Recovery on a Badland at *Sedebo* Study Site

Fig. 70:   Off-site Damages at *Sedebo* Study Site

Relief position of the badlands in the geomorphological unit *Valleys and Basin* is similar to the relief position of the badlands in the *Western Ethiopian Highlands,* but they also occur on grasslands (fig. 68, right picture).
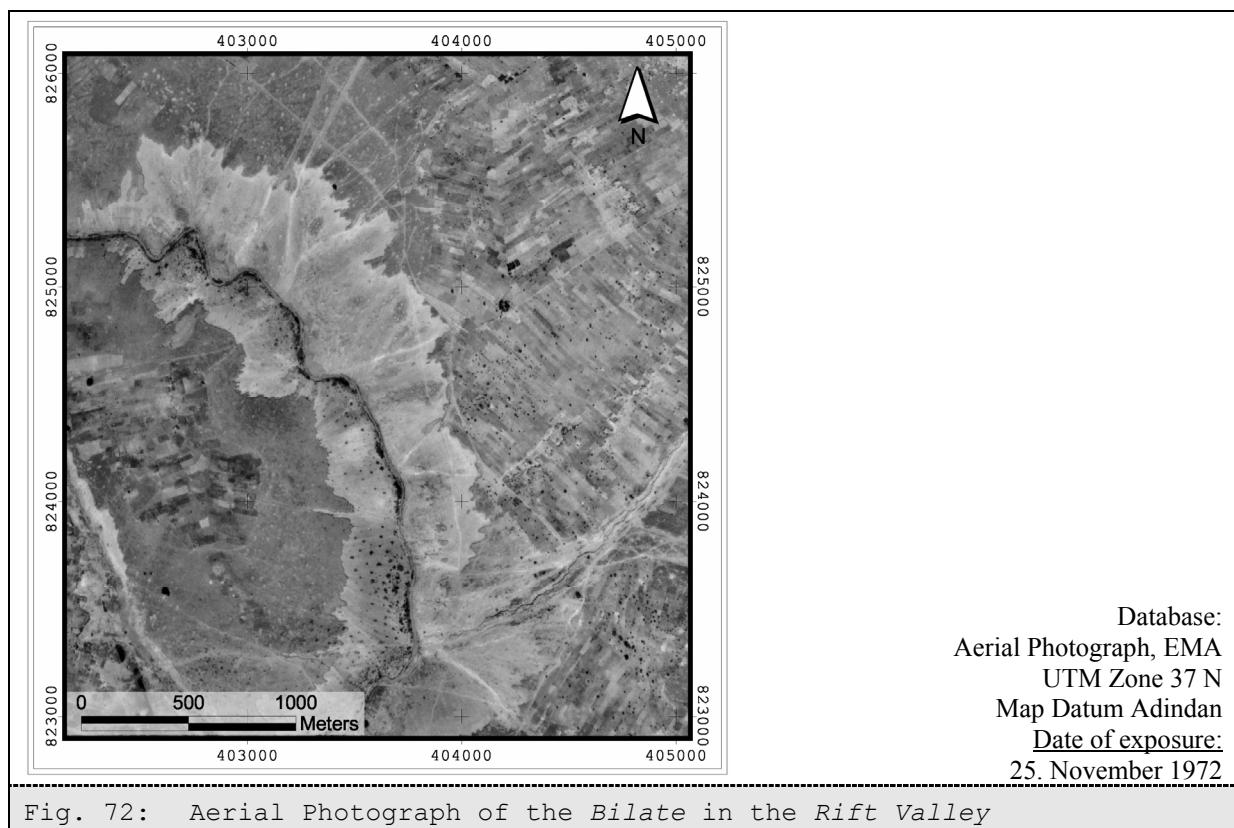
7.2.5   Barren Land Degradation

Barren degraded land occurs only in the *Rift Valley* and coincides with the development of gully systems. In the study area *Dimtu (RV)* hundreds of gullies have formed a barren area that is completely degraded. Soil and Saprolite have been washed out up to some 5 m in depth and secondary incisions into the erosion base are beginning to form. This barren area extends over ~4 km². The photographs (fig. 71 and 72) show the characteristic shape of the rim of the degraded land.

The main difference between badlands and the barren degraded areas is the gradient of the slopes **within** the rims. In the *Valleys and Basin* the gradient of the badlands never reaches more than 35° which is the maximum possible gradient of unconsolidated material. In contrast, slope gradients at the rims of the barren degraded land in the *Western Ethiopian Highlands* and in the *Rift Valley* are much steeper, sometimes reaching 90°.

Fig. 71:   Gully Concentration Developing a Barren Degraded Land

Where gullies occur in concentrated clusters degradation is permanent. These areas are located at similar relief positions and tend to have a same shape: their extent always follows a river and is related to the gradient of the slopes parallel to the river. These degraded areas develop where steep slopes are located very close to the channels and the relief curvature is convex. They reach a maximum depth of four m, because a concrete change of the petrography prevents deeper incision. Only in some regions do secondary incisions take place. The horizontal extents of barren land vary across the sites. Figure 73 shows the distance from the rim of the degraded land (light grey colour in photograph) to the channel of the *Bilate*. This variation ranges from 100 m to 800 m within a distance of two kilometres river length.

Database:
Aerial Photograph, EMA
UTM Zone 37 N
Map Datum Adindan
Date of exposure:
25. November 1972

Fig. 72:   Aerial Photograph of the *Bilate* in the *Rift Valley*

7.3   Soils and Soil Sediments
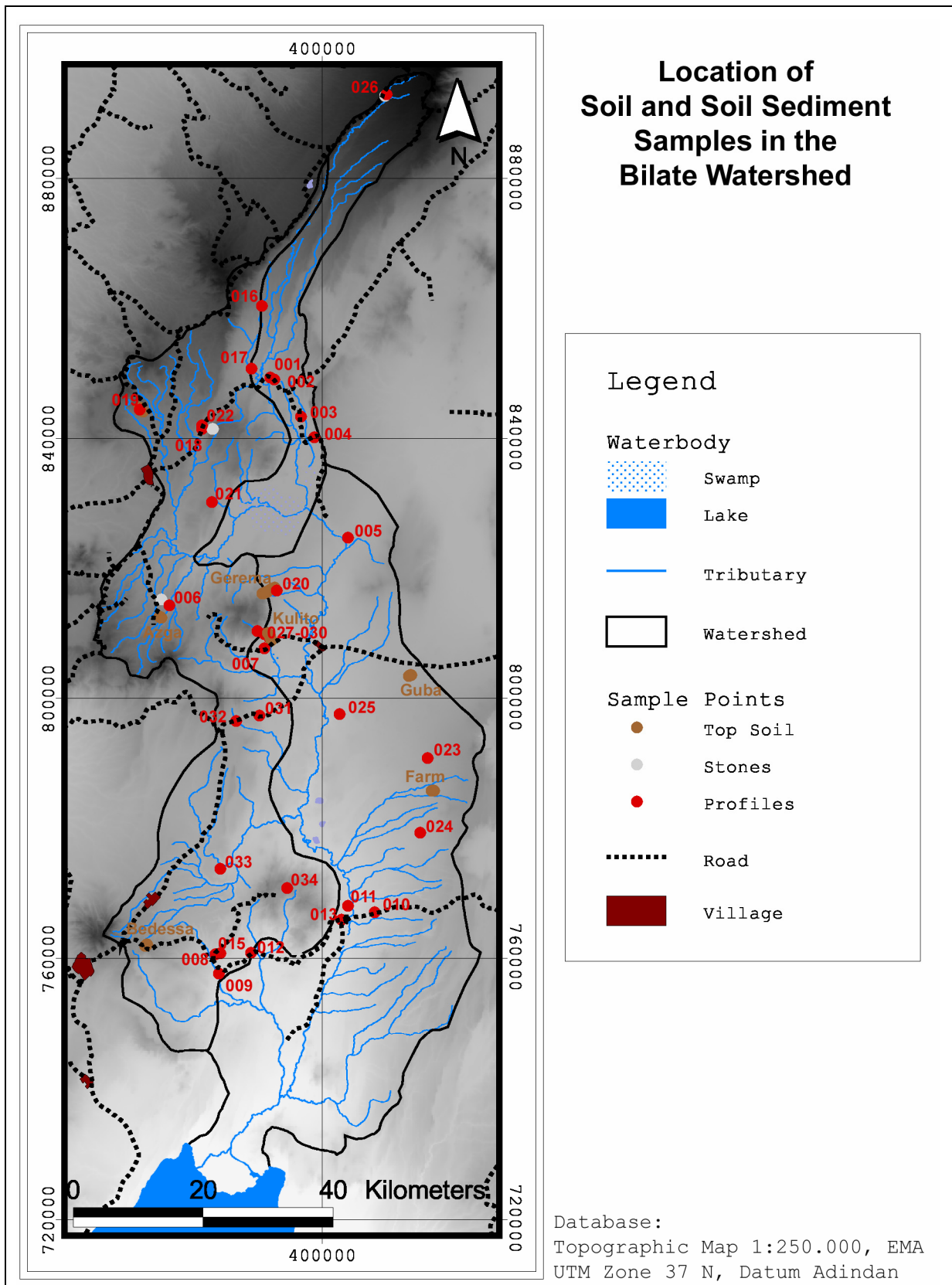
Fig. 73:   Location of Samples from Topsoils and Profiles

Table 17:	Vertical profiles: Location, Relief Properties and association to FAO Soil Unit					
Sample Number	Location (UTM) [easting/northing]	Altitude [m a.s.l.]	Slope [°]	Complex Curvature [profile curvature - plan curvature]	Flow-Accu [counted cells]	Soil Class [FAO-Unit]
VP 001	391811 / 849369	2,052	5.7	cx / pcx	1	Leptosols
VP 002	392432 / 849087	2,035	5.6	cx /pcx	3	Leptosols
VP 003	396533 / 843371	1,982	4.0	cv / pcv	3	Luvisols
VP 004	398597 / 840138	1,940	4.7	cx / pcx	0	Andosols
VP 005	403779 / 824750	1,881	4.5	cx / pcx	2	Andosols
VP 006	376350 / 814289	2,182	9.3	cx / pcx	1	Luvisols
VP 007	390938 / 807706	1,829	2.6	cx /pcx	5	Andosols
VP 008	383372 / 760628	1,650	3.8	str / pstr	0	Vertisols
VP 009	383958 / 757630	1,507	1.2	cv /pcv	3	Vertisols
VP 010	407872 / 767062	1,630	2.9	cx / pcx	3	Leptosols
VP 011	403780 / 768040	1,526	1.3	cv / pcv	0	Leptosols
VP 012	388897 / 760815	1,472	1.5	cx / pcx	0	Vertisols
VP 013	402833 / 765919	1,523	1.3	cv /pcv	5	Vertisols
VP 015	384191 / 760773	1,620	8.6	cx / pcx	3	Vertisols
VP 016	390545 / 860369	2,310	6.0	cx / pcx	0	Leptosols
VP 017	388972 / 850727	2,061	4.5	cx / pcx	0	Leptosols
VP 018	381359 / 841968	2,227	5.3	cv / pcv	22	Luvisols
VP 019	371802 / 844391	2,489	11.0	cx / pcx	13	Luvisols
VP 020	392861 / 816561	1,937	2.1	cv / pcv	14	Andosols
VP 021	382888 / 830225	2,199	5.7	cx / pcx	4	Nitisols
VP 022	381344 / 841381	2,215	3.5	cv / pcv	15	Luvisols
VP 023	416006 / 790794	1,939	2.1	cv / pcv	0	Andosols
VP 024	414874 / 779328	1,827	2.0	cx / pcx	5	Andosols
VP 025	402505 / 797549	1,740	1.4	cx / pcx	1	Andosols
VP 026	409725 / 892964	3,168	2.6	cx / pcx	5	Leptosols
VP 027	389883 / 810352	2,149	14.8	cv / pcv	2	Luvisols
VP 028	390948 / 809912	1,918	11.2	cx / pcx	0	Luvisols
VP 029	391499 / 809669	1,860	4.1	cv / pcv	33	Luvisols
VP 030	391791 / 809180	1,833	2.2	cx / pcx	1	Nitisols
VP 031	390147 / 797311	1,873	4.6	str / pstr	5	Nitisols
VP 032	386603 / 796479	1,943	4.3	cx / pcx	7	Nitisols
VP 033	384197 / 773758	1,843	3.8	cv /pcv	0	Nitisols
VP 034	394462 / 770796	2,155	8.8	cx / pcx	0	Luvisols

In the study area, 34 profiles were selected for sampling of soils or soil sediments (fig. 73). The profiles are located across the watershed and are allocated in correspondence with the occurrence of gullies, badlands or steep slopes truncated due to road construction. The

locations of the profiles have been selected first to correspond with the FAO soil classification system for easier comparison later on, second to investigate soil properties relevant for termination of soil erodibility. Table 17 lists the location of the profiles in UTM coordinates, altitude of the location point, inclination of the surrounding environment, relief element indicated by complex curvature, position within the relief indicated by the flow-accumulation and the spatial related FAO soil class.

The profiles are located at slope gradients between 1.3° and 14.8°, with most of the profiles being located on smooth to moderate slopes. Relief curvature is convex / plan convex for 17 profiles, concave / plan concave for 14 samples, and straight for two profiles. The flow accumulation is generally low, ranging from 0 to 7 [accumulated cells, cell size: 100 x 100 meter] for most locations. One flow accumulation cell represents 100 m slope length. Only the profiles VP 018, VP 019, VP 020 and VP 022 show flow accumulations between 13 and 33 [accumulated cells]. The association of relief properties at the sample sites to relief properties of specific soil types distinguished by the FAO soil classification could not always be verified. The exceptions are slope gradients and flow accumulation of sample locations that are linked to the FAO soil class Luvisols. All sample locations, which occur in areas of FAO soil class Luvisols, are located at relief elements of steep and long slopes. After FAO (1998) Luvisols are predominantly developed at such relief positions.

For detailed description of the profiles see chapter 14.2. In the following pages all investigated parameters of the profile's samples are also related to the FAO soil unit. This relation is only spatially caused but does not automatically associate the profiles (=soil type) to the specific FAO soil unit. It is only the spatial overlay and should help to verify the FAO soil unit data.

Measurements of samples' <u>colours</u> are expressed in the CIE colour system. For display purposes, this colour system was converted into RGB colours using the colourimetric conversion in Adobe Photoshop 7.0. The colours (fig. 74) of all samples show light grey to grey and light brown to brown shades. The colours of the samples within the FAO soil unit Leptosols and Andosols are all greyish, with the darker grey portions being located more at the top of the profiles and changing into lighter grey with increasing depth. The brownish colours from VP 016 and VP 017 are also brightening with increasing depth. No consistent system of colour distribution could be detected for the samples associated to the FAO Luvisols soil units. Across all depths, the colours range from light grey to dark brown, although they are generally darker than in the FAO Leptosols and Andosols soil units. No

data exist for the profile VP 029. Vertisols are brownish, except VP 009, in which grey is more pronounced. The profiles VP 008 and VP 015 show the typical horizon sequence of a Vertisol: darker colours on top are changing to slightly lighter colours towards the bottom of the profile. Most of these profiles have a depth of over 6 m. The colours of the samples within the FAO Nitisols soil units also range from grey to dark brown without a consistent pattern.

Fig. 74:   CIE Colours of Profile Samples
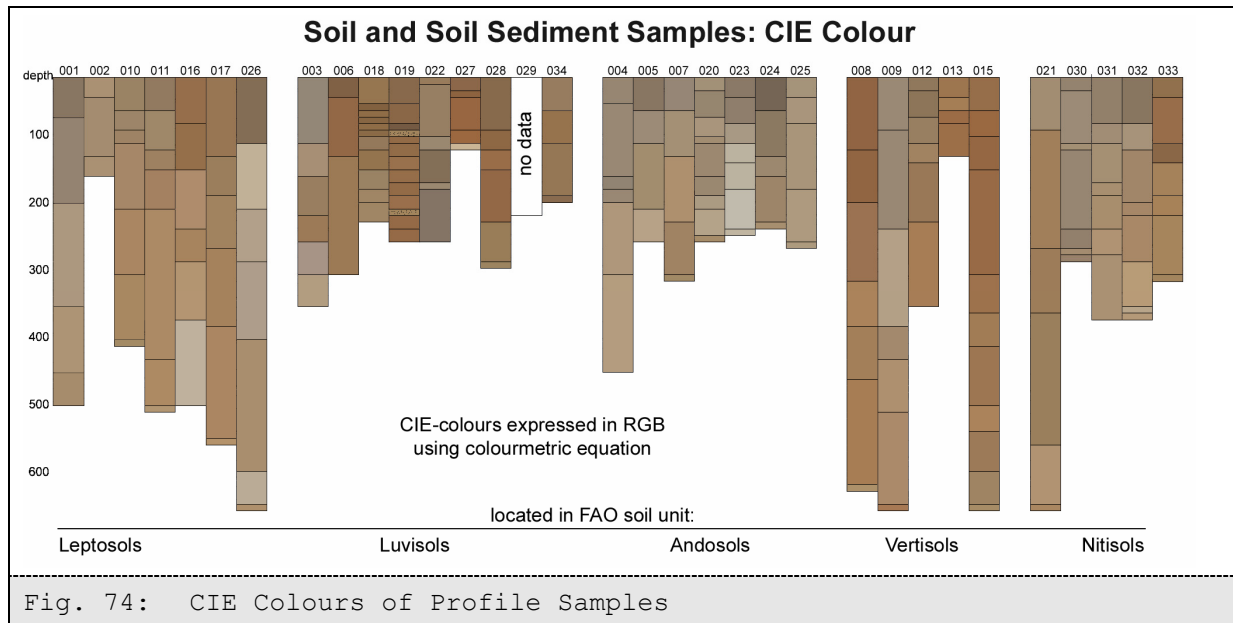
The <u>magnetic susceptibility</u> (fig. 75) of the samples ranges from 3.9 [μm³/kg] to 403.5 [μm³/kg] (mean=87.9, SD=78.2, n=235). The different values are illustrated from light (0-20 [μm³/kg]) to dark (180-200 [μm³/kg]) orange colour, while ruby colour indicates values greater than 200 [μm³/kg]. The susceptibility of the samples is low for the FAO Leptosols and Andosols soil units and consistently higher for FAO Luvisols, Vertisols and Nitisols soil units.

Fig. 75:   Susceptibility of Profile Samples
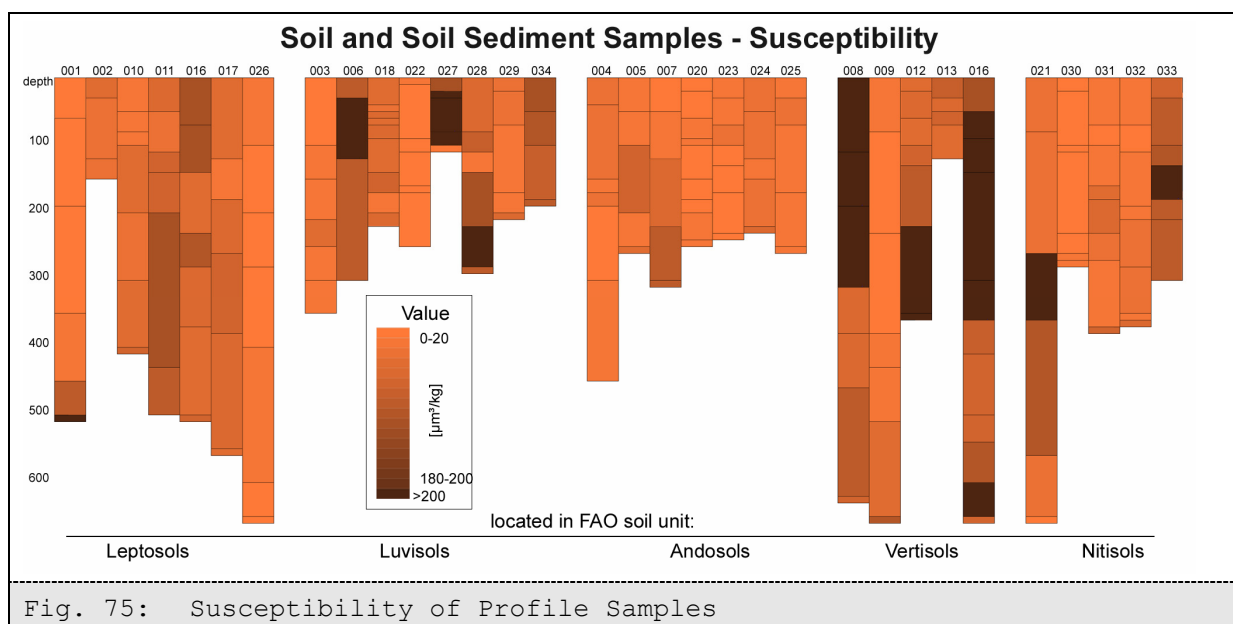
A correlation of susceptibility and CIE values is evident for samples associated to FAO Vertisols and Andosols soil units, but not for other profile samples and soil units. The high magnetic susceptibility of samples from VP 027 (FAO soil unit Luvisols) correlates to light brown CIE colours. In contrast, a sample in VP 006 shows high susceptibility and dark brown colour and again in VP 028 or VP 033 the correlation is indirect. The analysis did not determine a regular pattern of susceptibility for the samples in the vertical profiles.

Similarly, no clear pattern could be determined for the pH-values (fig. 76). These range from 4.2 [pH] to 7.5 [pH] (mean=5.1, SD=0.6, n=215). High and low pH values were detected without recognizable correlation to soil type or sample depth.
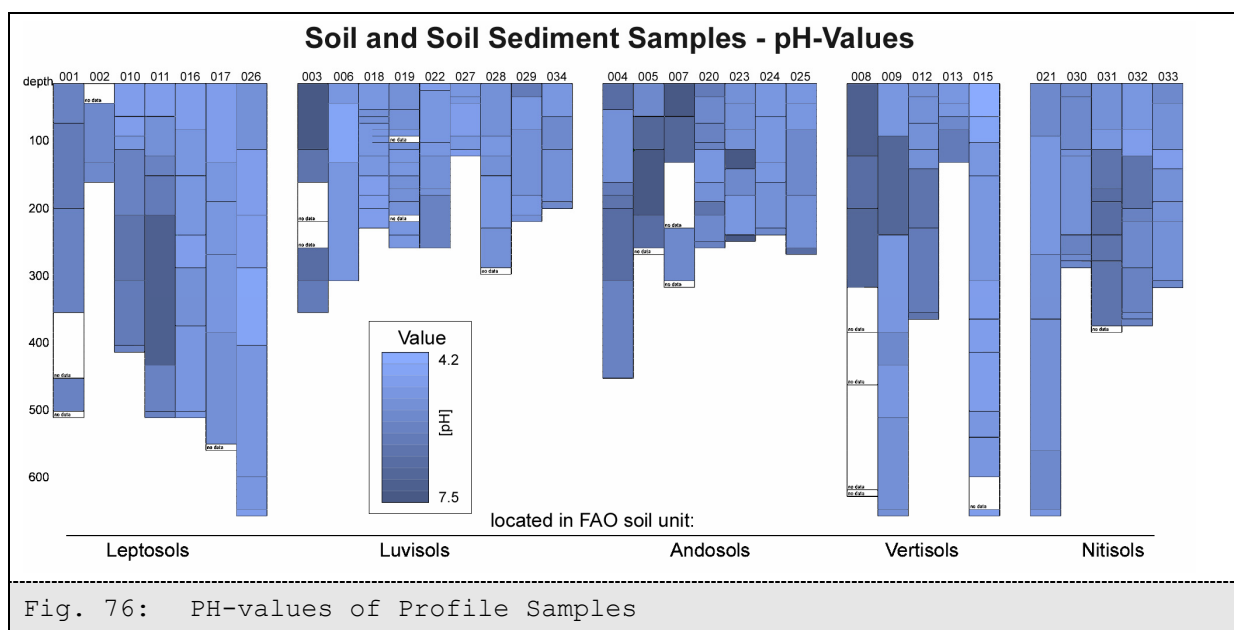
Fig. 76:   PH-values of Profile Samples
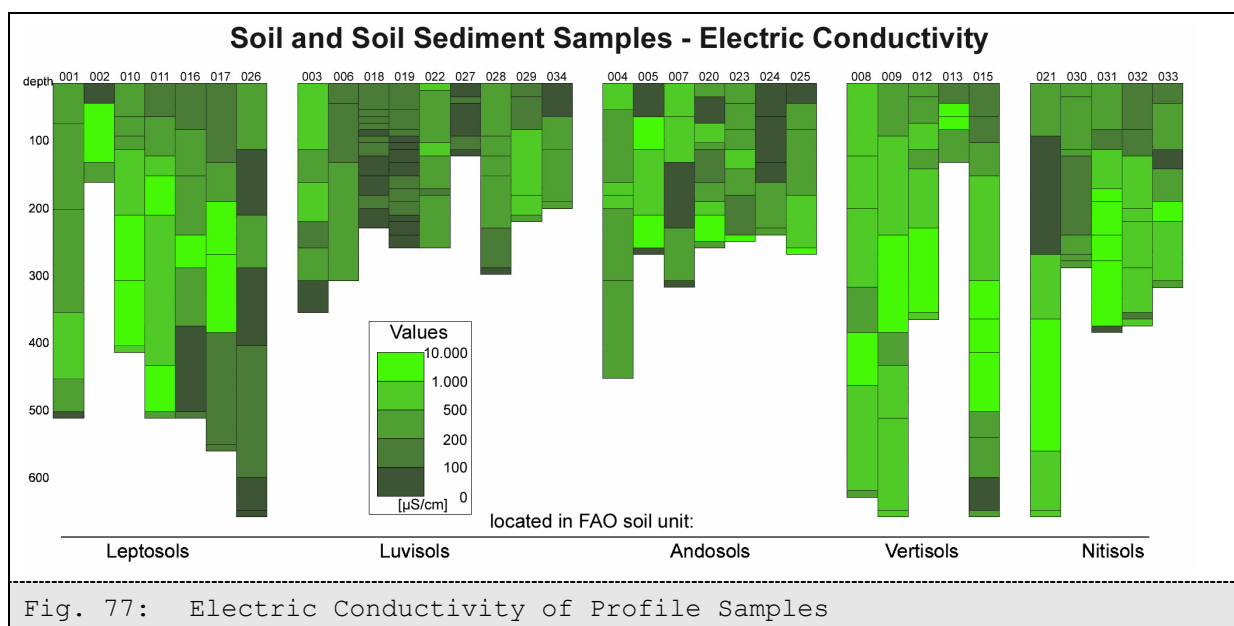
Fig. 77:   Electric Conductivity of Profile Samples

The electric conductivity (fig. 77) values range from 11.39 [µS/cm] to 7,244.46 [µS/cm] (mean=555.70, SD=817.24, n=219). The observed data illustrate higher electric conductivity for samples associated with FAO soil units Vertisols and, partially, Nitisols than those associated with FAO soil units Luvisols and Leptosol. Within the profiles, higher conductivity often occurs at deeper samples; top samples generally show lower electric conductivity.

Fig. 78:   Organic Carbon Content of Profile Samples
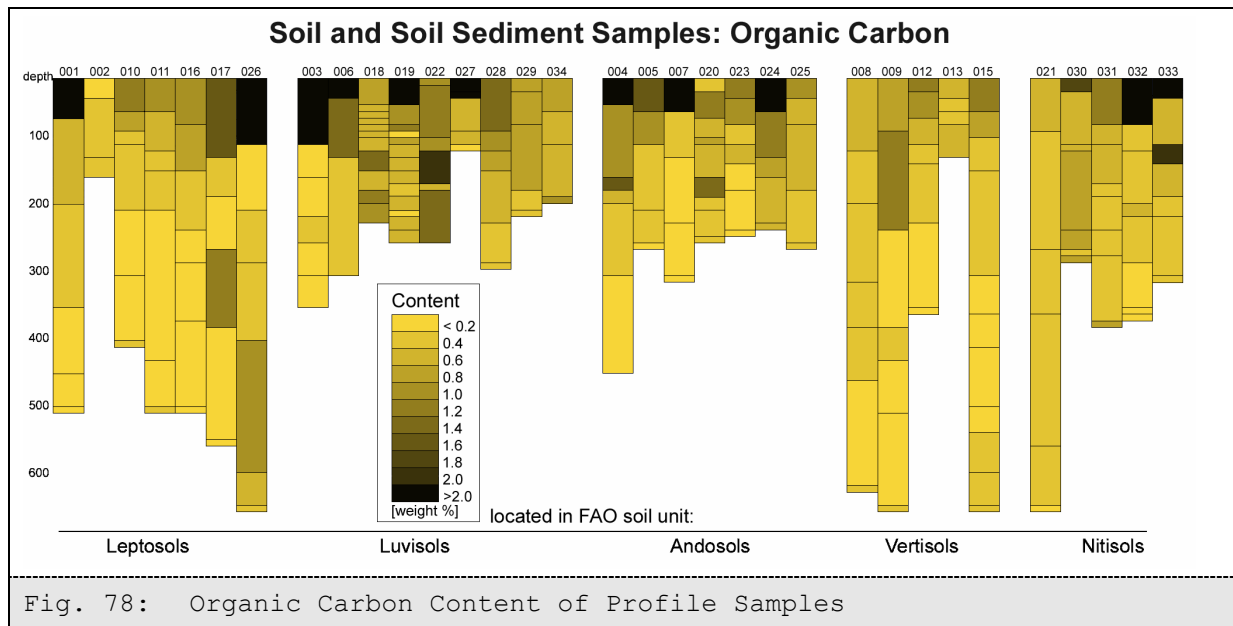
The organic carbon (C_{org}) content of the samples shows a typical vertical pattern with high content at the top and reducing with depth. The transition from A to B-horizon is concrete as the A-horizon has values higher two weight%. The highest C_{org} value of 6.45 [weight %] was measured at VP 026. This profile is located in the northern part of the *Valleys and Basin*. Other profiles with high organic carbon content in the top layers are spread across the watershed. Only profiles associated to the FAO soil unit Vertisols show smaller values of organic carbon content, whereas samples associated to FAO soil unit Luvisols generally seem to have higher C_{org} values (fig. 78).

The distribution of grain size within the samples is illustrated in two ways: first the sand fraction is displayed, then the clay content within the entire sample. The distribution of grain sizes of the sand fraction (fig. 79) shows no pattern within the soil groups. Fine sand dominates most profile samples, but within each profile no grading of the grain size distribution can be observed. There is some indication that profiles related to FAO soil unit Andosol show coarser grain sizes than profiles from other soil units. Moreover, the distribution pattern of the clay and silt content of each sample is random (fig. 80). Contents of clay and silt in profiles located in FAO soil unit Andosols are of smaller ratio than in the other

soil units. However, a grading could not be determined. A comparison of vertical profiles in different constellations and associations independent of the FAO soil classification yields similar results.
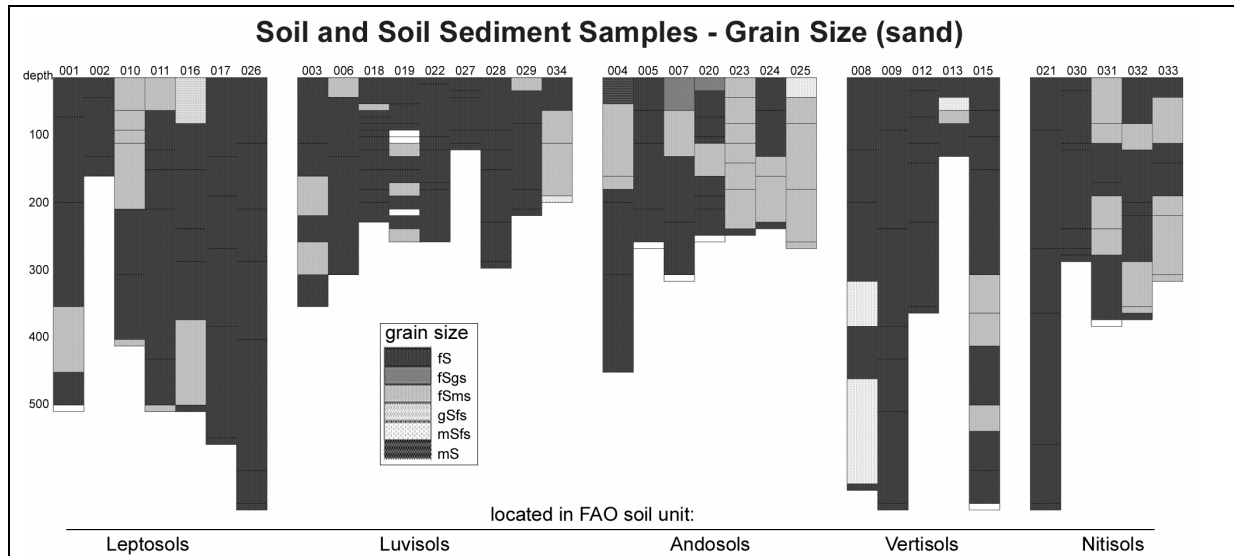

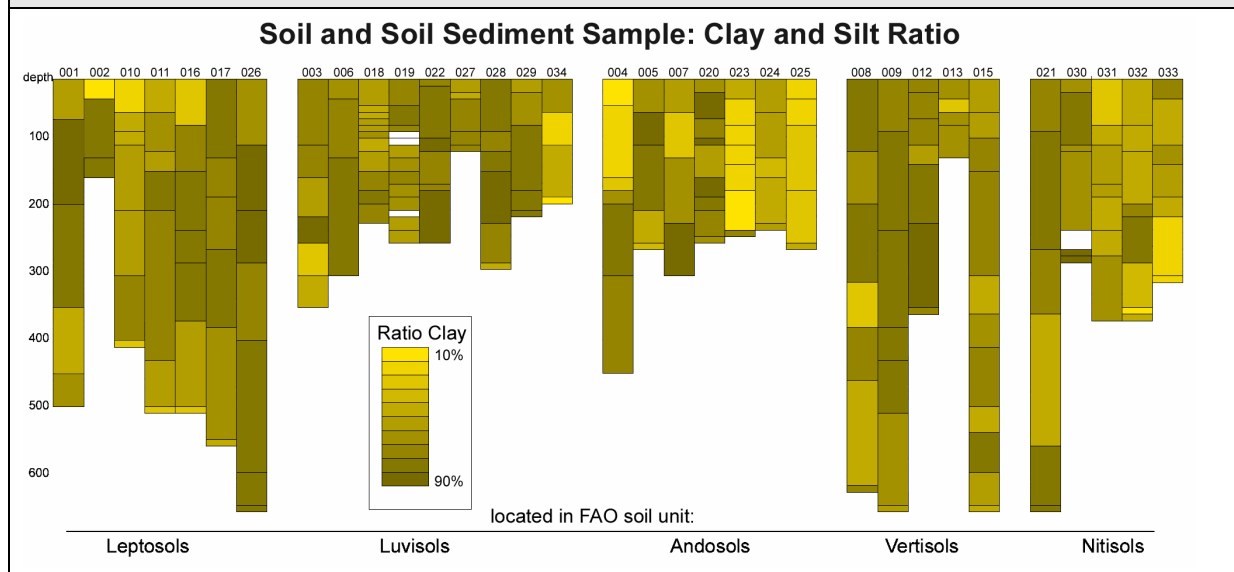Fig. 79:   Grain Size (Sand Fraction) of Profile Samples

Fig. 80:   Clay and Silt Ratio of Profile Samples

Clay minerals detected in the watershed are Allophane, Illite and Halloysite. Illite and Halloysite could only be found in very small ratios across the watershed, independently of sample location or soil profile depth. Allophane occurs in all samples and the ratio is much higher than for the other clay minerals. Figure 81 demonstrates the occurrence and the ratio of amorphous minerals: the subsurface is of smooth convex curvature with its zenith at 22° 2θ.

Fig. 81:   Mineralogical composition of VP032 2
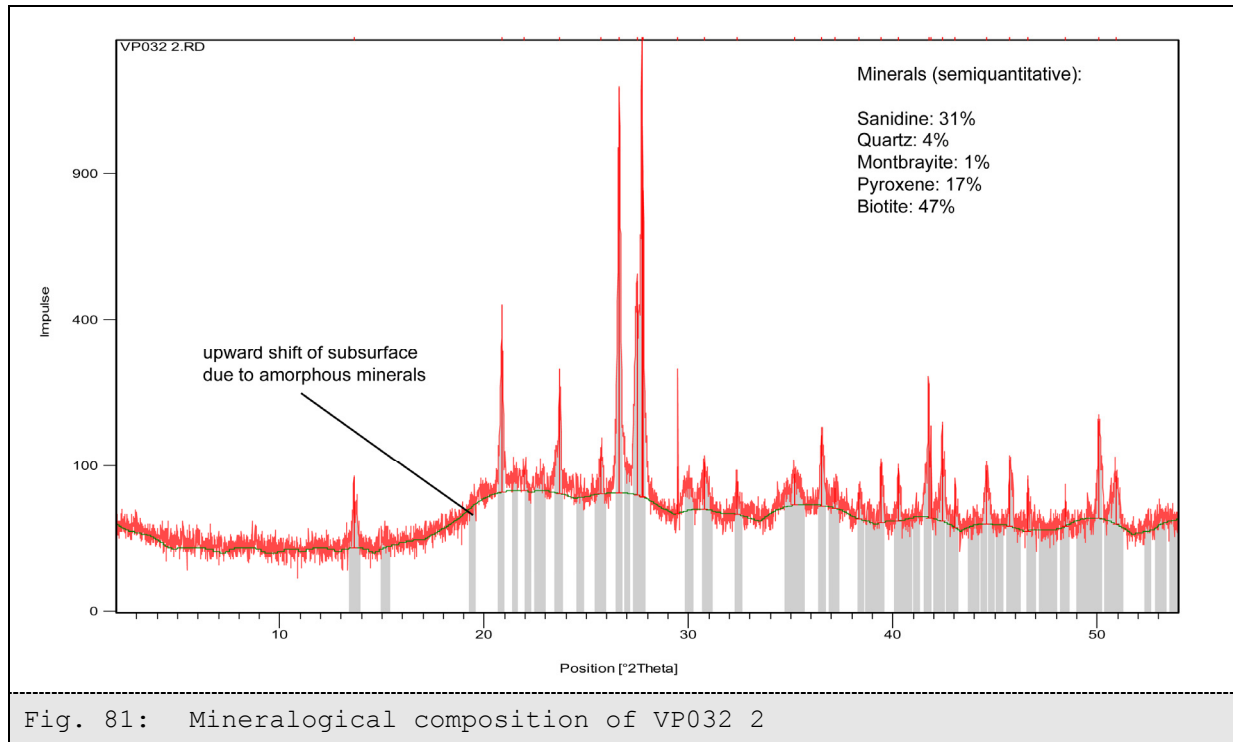
The high ratios of impulses of the subsurface are an additional indication that a relatively high amount of amorphous minerals, such as allophane, occur in this sample (fig. 81). All samples show more or less similar characteristics of the subsurface.

The mineralogy of soil and soil sediments is strongly linked to the prevailing bedrock. Thus, the mineralogy of the watershed does not vary to a great degree. The dominant geology is volcanic and pyroclastic bedrock and lacustrine sediments occur only in the southern part of the watershed in proximity to *Lake Abaya*. A semi-quantitative analysis of mineralogical composition is exemplarily reported for two profiles: VP 032 is located in the *Rift Valley* and VP 007 is located in the *Western Ethiopian Highlands*. Both profiles show high ratios of Pyroxene and small ratios of Quartz. Whereas feldspars are the dominant minerals in the *Rift Valley*, in the *Western Ethiopian Highlands* Anorthite are prevailing. Here, hematite could also be detected. In contrast, montbrayite is of higher ratio in the *Rift Valley* than in the *Western Ethiopian Highlands*. The occurrence of clay minerals could be detected, but due to the methodology of this analysis, only semi-quantitative ratios were estimated (Tab. 18).

Table 18: Mineralogical Composition of Profiles in the *Rift Valley* (VP 032) and in the *Western Ethiopian Highlands* (VP 007)						
Sample	Quartz	Feldspar	Pyroxene	Anorthite	Montbrayite	Magnetite	Clay Minerals
VP032 1	9	54	36		2		X
VP032 2	8	58	33		1		X
VP032 4	4	62	29		4		X
VP032 5	10	49	37		5		XX
VP032 6	9		84		3	4	XXX
VP032 7	12	34	45		9		X
VP032 8	7	26	63		3		XX
	Quartz	Hematite	Pyroxene	Anorthite	Montbrayite	Biotite	Clay Minerals
VP007 1	7	1	19	39			X
VP007 2	8	5	27	34		17	X
VP007 3	7	3	29	61			X
VP007 4	1		42	55	1		XX
VP007 5	2		47	50	1		

The results of the analysis of the profiles indicate only very little relation between the existing soils and the FAO soil units. For instance, the FAO data show soil units in the *Rift Valley*, which do not occur. Here, fotographs (see annex 14.2) of the profiles display clear an overlay of sometimes two soils: a buried soil covered by probably pyroclastic layers and a new developing soil on top. Similar sequence of layers was investigated in the *Valleys and Basin* as well as in some parts of the *Western Ethiopian Highlands*.

7.4   Land Cover

Table 19: Land Cover Class Index (LCCI)		
class 1	class 2	class 3
class 4	class 5	class 6

The Land Cover Class Index (LCCI) designed for this study is determined either visually or through remote sensing. The six classes determined through computer analysis and verified with ground data correspond to the vegetation characteristics listed in table 19.

Class 1 is dominated by very high perennial vegetation cover. Next to natural trees and small plantations, high densities of *ensete* or banana as well as coffee occur. Moreover, seasonal vegetation occurs on agricultural fields and often consists of agricultural crops, such as beans and maize. The class often alternates in time with the class 5, since vegetation cover on agricultural fields depends on agricultural calendars.
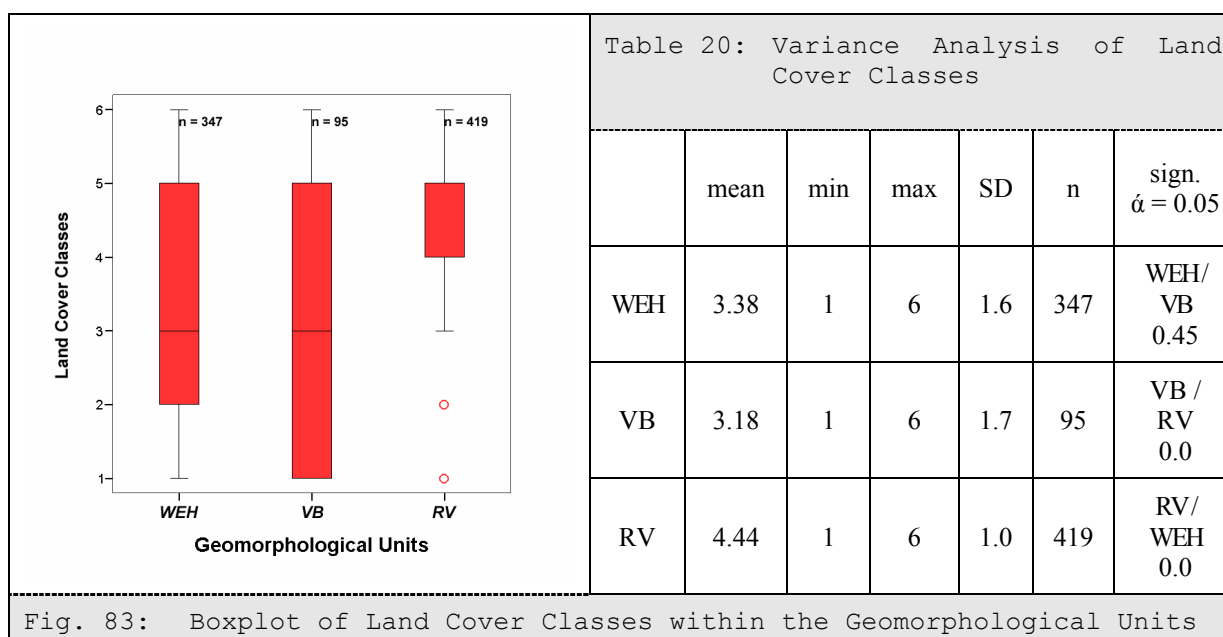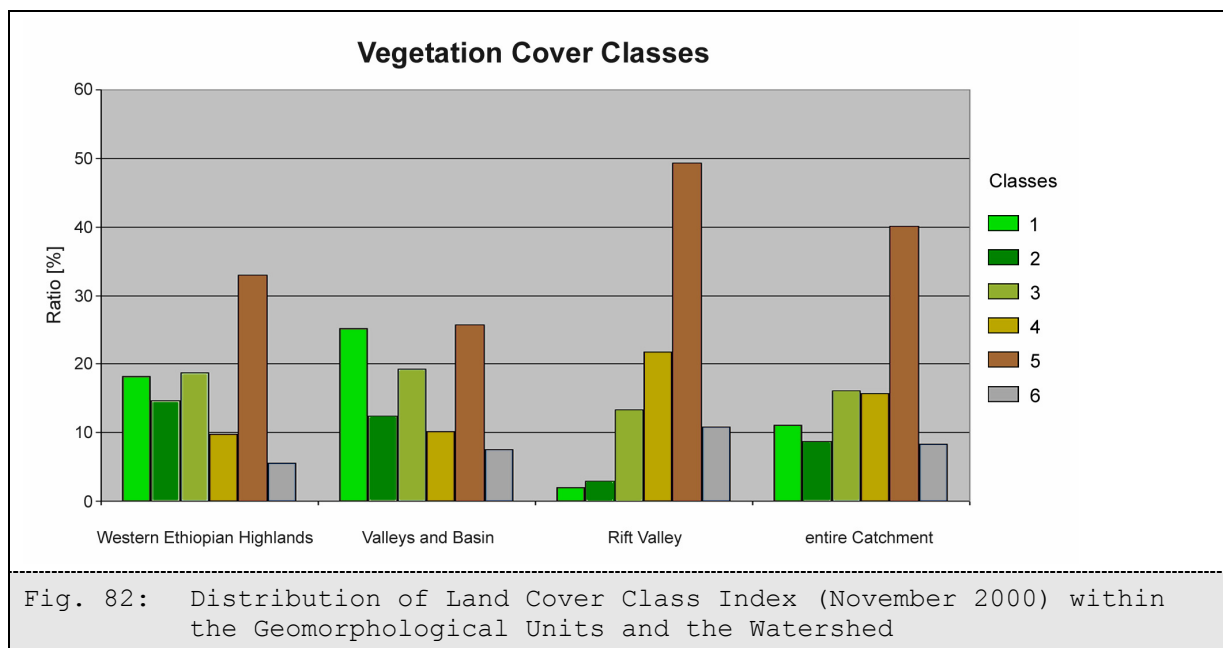
Class 2 represents perennial vegetation such as grassland and shrubs. Trees such as coniferous trees also exist within this class. The vegetation of this class is not of high chlorophyll content and thus the area-wide colour is not as intensively green as in class 1. In addition, grasslands in this class are usually over utilised for pasture and thus, vegetation is less active.

Class 3 is a mixture of bare or degraded soil, gullies or badlands with green vegetation interspersed. The vegetation typically consists of eucalyptus trees and shrubs, often in the form of reforestation measures. Intensive grazing prevents establishing of dense grass cover. Additionally, forests are very open and thus litter cover is rare.

Class 4 characterises degraded lands with only little vegetation cover. The vegetation type consists of grass or fallow land. Shrubs and isolated trees or open forests also occur in this class. However, vegetation in this class is rarely active.

Class 5 represents bare soil on agricultural fields. Thus, this class is usually found in association with class 1, which represents agricultural fields with active vegetation.

Class 6 represents all areas of barred degraded land. Degradation is advanced here; the surface is unconsolidated gravel or a highly weathered Saprolite complex that is often covered by a crust.

Fig. 82:   Distribution of Land Cover Class Index (November 2000) within the Geomorphological Units and the Watershed

Table 20: Variance Analysis of Land Cover Classes

	mean	min	max	SD	n	sign. $\acute{\alpha} = 0.05$
WEH	3.38	1	6	1.6	347	WEH/ VB 0.45
VB	3.18	1	6	1.7	95	VB / RV 0.0
RV	4.44	1	6	1.0	419	RV/ WEH 0.0

Fig. 83:   Boxplot of Land Cover Classes within the Geomorphological Units

Figures 82 and 84 illustrate the distribution of the land cover class index in the watershed. The classes 6 and 4 occur in all geomorphological units, but the classes 5 and 4 dominate in the *Rift Valley*. In contrast, the classes 1 and 2 are almost exclusively located in the *Western Ethiopian Highlands* and in the *Valleys and Basin*. The ratio for the land cover class 1 is highest in the *Valleys and Basin*, where it represents the dense and continuously green vegetation. In the *Western Ethiopian Highlands*, the class 5 has the highest ratio due to the date of the satellite images: the dry season.
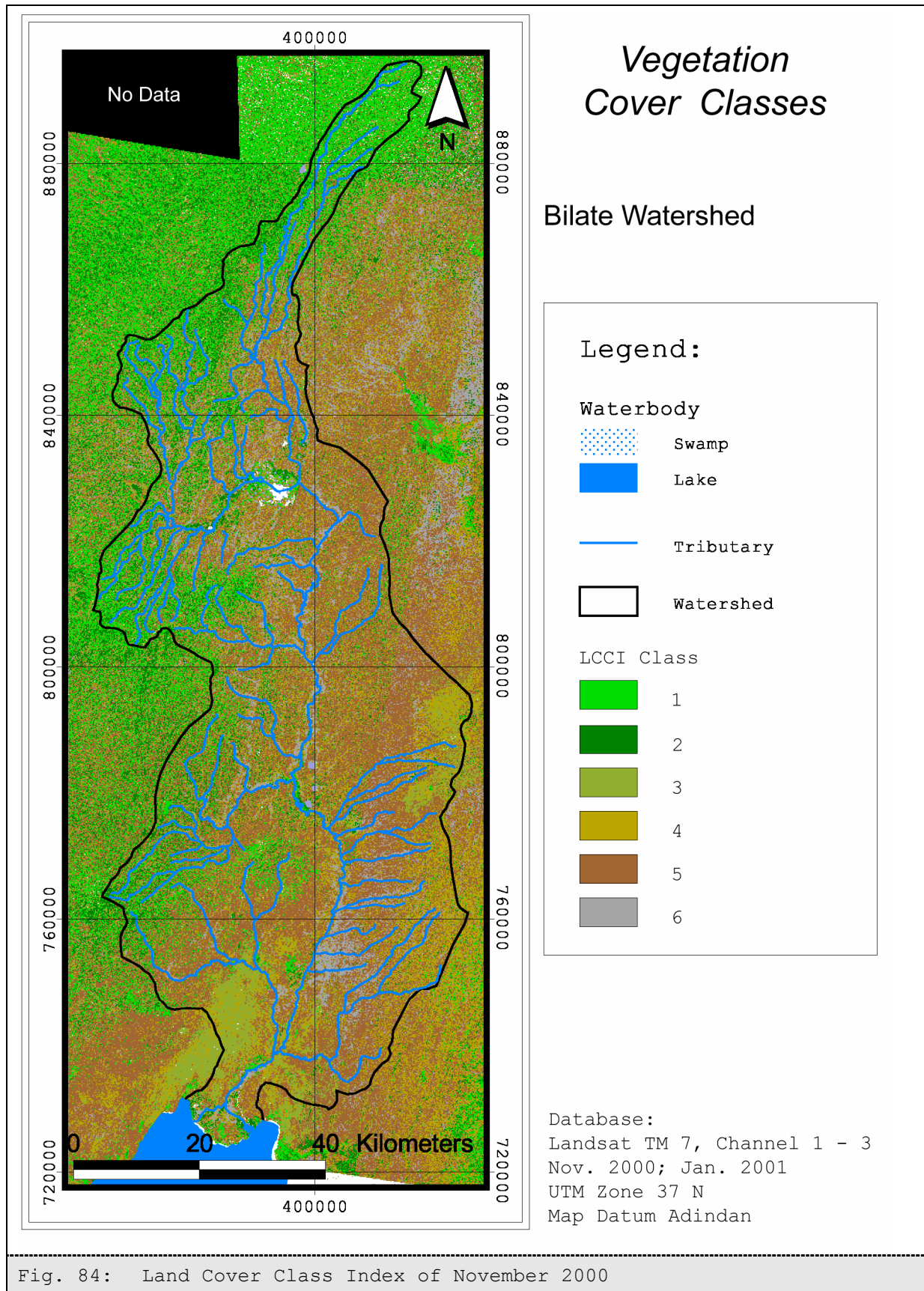
A variance analysis of the land cover class index verifies a significant difference between the *Western Ethiopian Highlands* and the *Valleys and Basin* in comparison to the *Rift*

Valley (fig. 84). Here, the land cover class 1 and 2 occur as exception only, whereas its mean is shifted strongly to the indexes of less vegetation (tab. 20). However, the differences of the index between *Western Ethiopian Highlands* and *Valleys and Basin* are not significant. The results indicate a slightly higher variance of vegetation in the *Valleys and Basin* than in the *Western Ethiopian Highlands*.

Next to the remote sensed investigation of the land cover, ground mapping broad information on land cover. In all geomorphological units a similar pattern was observed: movement of livestock and men destroy the vegetation cover parallel of footpaths. Intensive grasing of cattle and high movement of men in proximity to *tukuls* and watering places also lead to destruction of the vegetation cover. SCHÜTT & THIEMANN (2001) observed similar effects in watershed on northern Ethiopia. This very local observed change of vegetation cover was not investigated with the LCCI.

During all field trips an intra-annual change in vegetation cover was observed. This change is strongly linked to anthropogenic activities, such as agriculture, but also to alternating rainy and dry season. The intra-annual cycle can be describes as follows:

Table 21: Intra-annual vegetation cycle		
Month	**Vegetation cover**	
	-- little	++ high
Jan.	--	
Feb.	-	
Mar.	+	
Apr.	++	
May	+	
Jun.	+	
Jul.	+	
Aug.	++	
Sep.	++	
Oct.	0	
Nov.	-	
Dec.	-	

Fig. 84:   Land Cover Class Index of November 2000

The quality of the spatial distribution of the LCCI was verified by overlay of the LCCI on NDVI data from the same month. The spatial correlation is weak, due to the problem that more than appr. 1,089 LCCI cells are located within one NDVI cell. Figure 84 displays the freuquency of LCCI cells that occure in cells of same NDVI [number]. A general trend indicates a higher frequency of LCCI class six in cells of lower NDVI numbers than in cells of higher NDVI numbers. Similar trend can be observed with LCCI classes five and four. Contrary, the LCCI classe three to one examine higer frequencies in cells of higher NDVI numbers.

The visuall verification of the LCCI dataset by overlay on the NDVI dataset shows that the correlation is better in areas of little vegetation, such as in the *Rift Valley*, the lower parts of the *Valleys and Basin* and the lower regions of the *Western Ethioian Highlands* than in regions with higher vegetation cover like in the higher regions of the *Western Ethiopian Highlands*, *Valleys and Basin* and on the volcanoes.

Any multitemporal analysis was not carried out, since the high cloud cover during rainy season prevents analysis of remote sensed ground data.

Fig. 85: LCCI versus NDVI for January